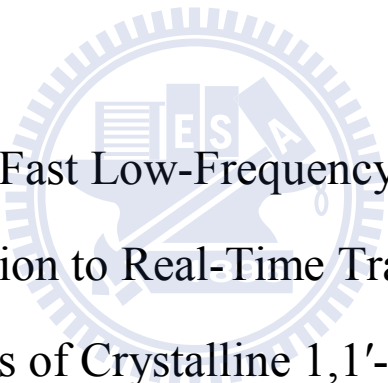


國立交通大學

應用化學系碩士班

碩士論文

架設快速低振動頻率的拉曼光譜儀
並應用於即時監控結晶態1,1'-binaphthyl的熔化過程



Construction of a Fast Low-Frequency Raman Spectrometer
and Its Application to Real-Time Tracing of the Melting
Process of Crystalline 1,1'-binaphthyl

研究生：王偲丞

指導教授：重藤真介 博士

中華民國一百年八月

架設快速低振動頻率的拉曼光譜儀
並應用於即時監控結晶態1,1'-binaphthyl的熔化過程

研 究 生：王僊丞

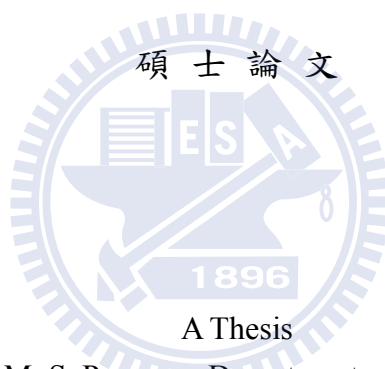
Student：Szu-Cheng Wang

指導教授：重藤真介 博士

Advisor：Dr. Shinsuke Shigeto

國 立 交 通 大 學

應用化學系碩士班



Submitted to M. S. Program, Department of Applied Chemistry
College of Science
National Chiao Tung University
in Partial Fulfillment of the Requirements
for the Degree of
Master
in
M. S. Program, Department of Applied Chemistry

August 2011

Hsinchu, Taiwan, Republic of China

中華民國一百年八月

架設快速低振動頻率的拉曼光譜儀 並應用於即時監控結晶態1,1'-binaphthyl的熔化過程

學生：王偲丞

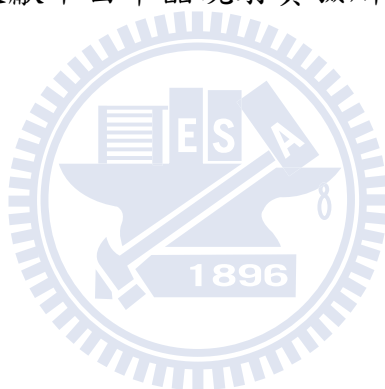
指導教授：重藤真介 博士

國立交通大學應用化學系碩士班

摘要

研究凝態物質的分子間作用力和晶格振動可以藉由低頻率(小於 200 波數)拉曼光譜學，但此技術的困難在於雷利散射比所要的拉曼訊號強上幾個級數。市面上典型的 notch 濾片無法有效的過濾雷利散射，因此要得到 200 波數以下的拉曼訊號相當困難。雖然單通道偵測器結合三分光儀(triple monochromator) 可以有效的分離雷利散射和拉曼散射並得到低頻率(小於 50 cm^{-1})且高訊雜比的拉曼光譜圖，但如果研究相變化這類型的動力學過程，多通道的偵測器才有辦法以較短的曝光時間(小於 1 秒)完成測量。在本論文中我們使用充滿碘蒸氣的玻璃槽做為消除雷利散射的濾片並結合多通道的拉曼光譜儀，我們能夠以小於 1 秒的測量時間記錄 10 波數以下的史托克斯和反史托克斯的拉曼訊號。接著將此低振動頻率拉曼系統應用到結晶態 1,1'-binaphthyl。這個分子在結晶態有兩個晶型：類順式與類反式，並有著不同的熔點。我們發現兩個晶型在低頻率範圍(-200 — $+200\text{ cm}^{-1}$)呈現截然不同的拉曼光譜。為了瞭解低振動頻率訊號的來源，快速的加熱樣品並以 0.2

秒的測量時間記錄每一張光譜圖，由此觀察兩個晶型的拉曼光譜隨溫度的變化。除此之外，藉由史托克斯和反史托克斯譜帶強度的比率，每個數據點的樣品溫度可以高精準度的被估計。將這兩組溫度變化的拉曼光譜數據搭配理論計算的結果，我們推測類反式中的 26 cm^{-1} 峰和類順式中的 100 cm^{-1} 峰分別是碳碳單鍵的扭曲振動和平面外變形振動(分子內振動)。由於分子間的作用力與熱膨脹造成低振動頻率波帶往低頻率位移有關，實驗得知類反式的拉曼波帶位移的程度較類順式少，因此我們認為類反式的分子間作用力較類順式強，而文獻中由單晶繞射實驗所得到的結果與我們的推測吻合。



Construction of a Fast Low-Frequency Raman Spectrometer and Its Application to Real-Time Tracing of the Melting Process of Crystalline 1,1'-binaphthyl

Student: Szu-Cheng Wang

Advisor: Dr. Shinsuke Shigeto

M. S. Program, Department of Applied Chemistry

National Chiao Tung University

Abstract (in English)

Low-frequency ($<200\text{ cm}^{-1}$) Raman spectroscopy enables us to investigate intermolecular vibrations and lattice vibrations in condensed phase materials. However, low-frequency Raman signals can be almost completely buried under vast Rayleigh scattering. Typical commercial notch filters are not effective enough to eliminate Rayleigh scattering and do not allow us to reach the frequency region below 200 cm^{-1} . Moreover, in order to keep track of dynamic processes such as phase transitions, multichannel detection rather than single-channel detection with a double/triple monochromator is required. In this work, by combining an I_2 vapor-containing cell as a Rayleigh rejection filter with a multichannel Raman spectrometer, we have successfully recorded Raman spectra down to $\sim 10\text{ cm}^{-1}$ in both Stokes and anti-Stokes sides simultaneously. The constructed Raman spectrometer has then been applied to crystalline 1,1'-binaphthyl, which has two different crystal polymorphs, that is, the cisoid and transoid forms. They show quite distinct spectral features in the low-frequency region (-200 – $+200\text{ cm}^{-1}$). Real-time tracing of the melting process of two crystalline forms have also been conducted with rapid heating. A series of Raman spectra have been recorded every 0.2 sec, in which spectral changes of low-frequency bands are clearly observed. In addition, the sample temperature has been accurately estimated from the Stokes/anti-Stokes intensity ratio of the Raman bands. Base on the temperature-dependent Raman spectra and theoretical calculations, the 26 cm^{-1} band of the transoid form and the 100 cm^{-1} band of the cisoid form are assigned to the torsional vibration and out-of-plane deformation of the C–C single bond, respectively. Moreover, the peak position of each low-frequency band has been determined from the fitting. We found that peak shifts due to thermal expansion for the transoid form are smaller than those for the cisoid form. Thus, intermolecular interactions in the transoid form are stronger compared with those in the cisoid form. This finding is consistent with their X-ray crystal structures.

Acknowledgments

My deepest gratitude goes first and foremost to Professor Shigeto, my supervisor, for providing me an opportunity for studies in this thesis. His continuing encouragements and excellent guidance help me a great deal. Without his consistent and illuminating instruction, this thesis could not have reached its present form.

I would like to express my heartfelt gratitude to Professor Hamaguchi, who led me into the world of Raman spectroscopy. I am also greatly indebted to Doctor Yabumoto, who have instructed and helped me a lot in the past two years.

I also owe my sincere gratitude to my friends (Tsung-wei, Je-hau, Jian-jung,) and all members in Shigeto group who gave me their help and time in listening to me and helping me work out my problems during the difficult course of the thesis. And I am deeply grateful to Mr. Sudhakar for his kind assistances in chemical syntheses.

Last my thanks would go to my beloved family for their loving considerations and great confidence in me all through these years. Without their sincere supports, I could not have accomplished this work.

Tables of Contents

	Page
Abstract (in Chinese)	i
Abstract (in English)	iii
Acknowledgments.....	iv
Tables of Contents.....	v
List of Figures and Tables	vii
Chapter I General Introduction.....	1
I-1. Motivation of this study	2
I-2. Raman measurements of low-frequency motions	2
I-3. Multichannel detection in Raman spectroscopy.....	3
I-4. Vapor filters for Rayleigh scattering elimination	5
I-5. Content of this thesis	7
Chapter II Construction of a Fast Multichannel Low-Frequency Raman Spectrometer	8
II-1. Introduction	9
II-2. Multichannel low-frequency Raman spectrometer using a single-mode Ar-ion laser (514.5 nm) and I ₂ vapor filter	12
II-2-1. Experimental setup	12
II-2-2. Results and Discussion	16
Chapter III Real-Time Tracing of the Melting Process of the Two Distinct Polymorphs of Crystalline 1,1'-Binaphthyl	27
III-1. Introduction	28
III-2. Experimental.....	31
III-3. Results	33
III-4. Fitting analysis.....	39
III-5. Discussion: Temperature change during the melting	44
III-6. Discussion: Changes in Low-frequency Raman bands change during heating	48
III-7. Discussion: Possible vibrational mode of 26 cm ⁻¹ band in the transoid form and 100 cm ⁻¹ band in cisoid form	52
III-8. Torsional motions of other crystalline aromatic compounds.....	54

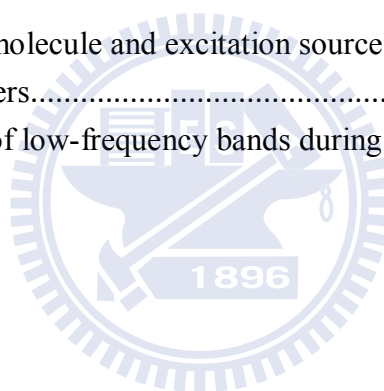
Chapter IV Conclusion.....	56
References	59



List of Figures and Tables

	Page
Figure I-1. Transmittance spectrum of a commercially available notch filter	4
Figure II-1. Laser gain curve and cavity modes of an Ar-ion laser.	9
Figure II-2. Calculated absorption lines of I ₂ in the visible frequency region accessible by (a) Ar-ion (514.5 nm), (b) Nd:YAG (532.0 nm) lasers.....	11
Figure II-3. Iodine vapor filter used in the present study.....	12
Figure II-4. Temperature dependent of iodine vapor pressure in the gas–solid equilibrium. .	13
Figure II-5. Photographs of the I ₂ vapor filter were taken at different filter temperatures (a) 24 °C (room temperature) (b) 95 °C.....	14
Figure II-6. Schematic diagram of a single longitudinal mode Ar-ion laser.	15
Figure II-7. Schematic diagram of the multichannel low-frequency Raman spectrometer. ...	16
Figure II-8. Intensity correction of the Raman spectrum of CCl ₄	18
Figure II-9. Raman spectra of L-cystine.....	21
Figure II-10. L-cystine Raman spectra in the low-frequency region.	22
Figure II-11. Comparison of the Raman spectra of L-cystine measured with three different filters.....	23
Figure II-12. Raman spectra of L-cystine obtained in the following two situations: (a) The laser light reflected by the glass capillary came into the I ₂ vapor filter (b) The reflected laser light was blocked by the 5 mm aperture	25
Figure II-13. Raman spectra of L-cystine measured by tuning the frequency of the single-mode Ar-ion laser.	26
Figure III-1. Axial chirality of 1,1'-binaphthyl.	28
Figure III-2. Schematic diagram of the two crystal forms of 1,1'-binaphthyl.	29
Figure III-3. Purification of commercially obtained 1,1'-binaphthyl and preparation of (a) cisoid form and (b) transoid form.....	31
Figure III-4. Photograph of the heating apparatus	32
Figure III-5. Raman spectra of the two forms of crystalline 1,1'-binaphthyl.	33
Figure III-6. Low-frequency Raman spectra of two crystalline 1,1'-binaphthyl.	34
Figure III-7. Low-frequency Raman spectra of the transoid form with rapid heating.	37
Figure III-8. Low-frequency Raman spectra of the cisoid form with rapid heating.	38
Figure III-9. Experimental data (red closed circles) of the transoid form and their fitted results (blue solid lines).	42
Figure III-10. Experimental data (red closed circles) of the cisoid form and their fitted results (blue solid lines).	43
Figure III-11. Plot of the estimated temperature versus heating time for the cisoid form.....	44
Figure III-12. Differential scanning calorimetry (DSC) measurements of cisoid form	

crystal with different heating rates.....	45
Figure III-13. Plot of the estimated temperature versus heating time for the transoid form. .	46
Figure III-14. Differential scanning calorimetry (DSC) measurements of transoid form crystal with different heating rates.....	47
Figure III-15. Plot of the peak positions of the seven low-frequency Raman bands against heating time.	49
Figure III-16. Plot of the peak positions of the seven low-frequency Raman bands against estimated temperature. (a) Transoid form and (b) cisoid form.....	50
Figure III-17. The crystal structures of the two forms of 1,1'-binaphthyl.	51
Figure III-18. The intramolecular vibrations in gas phase 1,1'-binaphthyl molecule calculated from density functional theory.	53
Figure III-19. Raman spectra of aromatic compounds containing the torsional motion.	55
Table I-1. Absorbing atom/molecule and excitation source combinations.....	5
Table III-1. Fitting parameters.....	40
Table III-2. The peak shift of low-frequency bands during heating.....	48



Chapter I

General Introduction



I-1. Motivation of this study

How can we understand crystal structural changes upon heating from the molecular viewpoint? Differential scanning calorimetry (DSC), which is a widely used technique in thermodynamic studies, can trace the free energy changes of materials and provides us with macroscopic understandings of phase transitions such as melting or crystallization processes [1, 2]. For further understanding of dynamical and microscopic aspects of these phase transitions, elucidation of the loss of a crystal structure and associated changes in intermolecular interactions during the melting process is deemed necessary. The purpose of the present study is to construct a spectroscopic apparatus that enables us to rapidly (<1 sec) monitor changes in intermolecular interactions and thereby deepens our understanding of phase transition at the molecular level.

I-2. Raman measurements of low-frequency motions

Intermolecular forces in molecular assemblies are reflected in intermolecular and/or collective motions. The frequency of these motions is usually smaller than 200 cm^{-1} (6 THz or 20 meV) and is observed in the low-frequency region of an optical spectrum. Measurements of Raman scattering in the frequency region below 200 cm^{-1} have been used for investigating the intermolecular and/or collective motions of materials in the condensed phase. For example, the optically active lattice vibrations, which correspond to the optical phonon modes at $\mathbf{k} = 0$ [3, 4], are observed below 500 cm^{-1} for alkali halides [5]. Similarly, the phonon modes of aromatic hydrocarbon crystals are observed below 150 cm^{-1} , corresponding to librational lattice vibrations. The intermolecular vibrations of water are detected at $780, 450, 175,$ and 60 cm^{-1} due to hydrogen bonding interactions [6].

These low-frequency motions were conventionally studied with a scanning Raman spectrometer, which is composed of a large multiple monochromator and a single-channel detector such as a photomultiplier tube (PMT) [7]. More recently, the progress in ultrafast lasers has enabled the measurement of low-frequency Raman spectra in the time-domain by using the optical Kerr effect (OKE) [8, 9]. Both these spectroscopic techniques employ the single-channel detection for obtaining a spectrum. It needs to scan the grating of a monochromator or to change the time delay in a step-by-step fashion. The single-channel detection is not suitable for measuring a rapidly changing substance, because it cannot simultaneously detect a wide range ($>1000\text{ cm}^{-1}$) of a spectrum and requires a long time for obtaining the whole spectrum.

The low-frequency motions, especially phonon modes in crystals, are also measured by far-IR (or THz) spectroscopy [10, 11], hyper-Raman spectroscopy [12-15], and neutron inelastic scattering [16]. Far-IR spectroscopy, both in the frequency-domain and the time-domain, employs the single-channel detection. Although hyper-Raman and neutron scattering can be detected by a multichannel detector, they need a very long acquisition time due to the small scattering cross sections. Thus, it is not easy to apply these techniques to the fast tracing of low-frequency motions.

I-3. Multichannel detection in Raman spectroscopy

There is no doubt that the use of an optical multichannel detector such as a charge coupled device (CCD) camera is one of the greatest innovations in Raman spectroscopy [17]. Multichannel detectors have more advantages compared with single-channel detectors in Raman spectroscopic measurements. They enable us to detect spatially dispersed signals simultaneously without scanning the grating of a spectrograph. A wide range of Raman

spectrum can be recorded in a short exposure time (<0.1 sec) with high spectral reproducibility. Furthermore, because the fluctuation of the excitation laser does not affect the observed spectra, the relative band intensities in the Raman spectra are highly reliable. If one can fully utilize the advantages of multichannel detection, Raman spectra of a short-lived transient species may be obtained.

In order to apply the multichannel detection technique to low-frequency Raman spectroscopy, immense Rayleigh scattered light should be selectively reduced. Typically commercial notch filters have a broad Rayleigh band rejection of >200 cm^{-1} (figure I-1). It rejects not only Rayleigh scattering but also low-frequency Raman scattered signals.

A number of studies related to multichannel low-frequency Raman measurements with the use of narrow bandwidth or sharp cutoff Rayleigh scattering elimination filters have been reported recently. Using multiple holographic notch filters [18] and a chevron-type dielectric filter [19] enable Raman measurements down to 28 cm^{-1} and 20 cm^{-1} , respectively. A

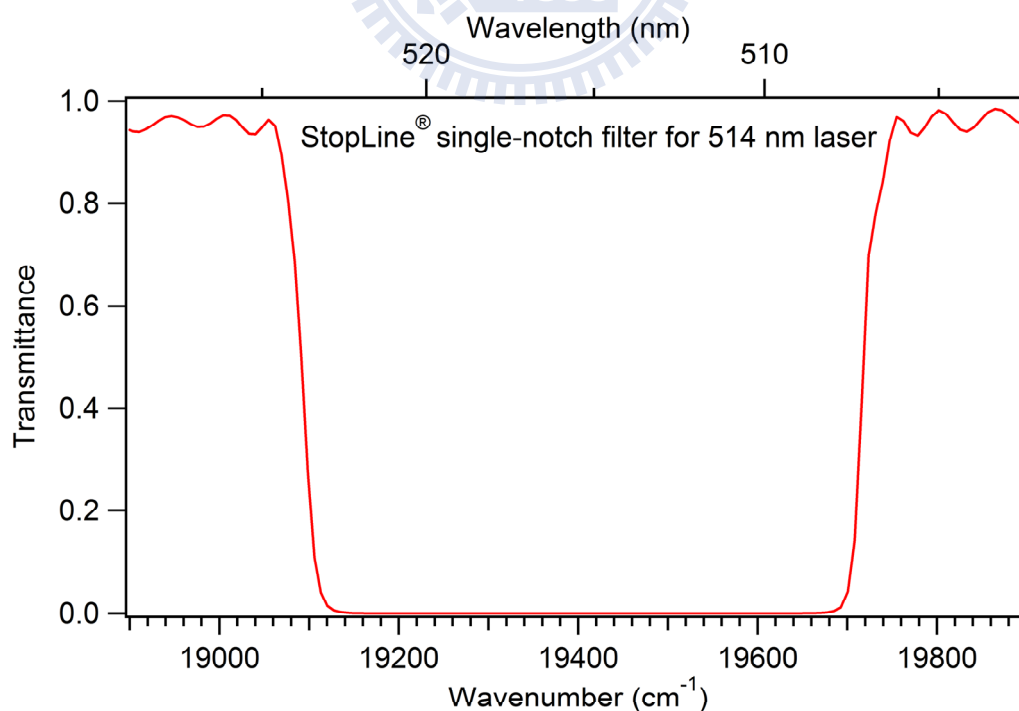


Figure I-1. Transmittance spectrum of a commercially available notch filter
(StopLine single-notch filter for 514.5nm excitation purchased from Semrock)

multichannel Raman spectrometer with a zero-dispersion double grating filter could measured a Raman spectrum down to 5 cm^{-1} [20], but only the Stokes side of the spectrum was recorded.

II-4. Vapor filters for Rayleigh scattering elimination

Absorption bands of atomic or molecular vapor have been used for eliminating strong Rayleigh scattering (table I-1). The Rayleigh scattering elimination efficiency of these bands is as high as 10 O.D. with Doppler-limited narrow bandwidth. If a certain vapor absorption band has exactly the same wavelength as that of the excitation light, it can be regarded as an ultra “notch” filter. The use of a vapor filter was first reported by Rasetti in 1930 [21]. The author used mercury vapor for eliminating the Raman excitation light, which was the 253.7 nm resonance line of a mercury arc lamp. After the development of laser Raman spectroscopy, many other vapor filters were combined with various lasers for this purpose.

Table I-1. Absorbing atom/molecule and excitation source combinations

Atom or Molecule	Wavelength (nm)	Excitation source
Hg	253.7	Mercury arc [25], Frequency-doubled dye laser [36]
Pb	283.3	Frequency-doubled dye laser [22]
Cs	388.9	Frequency-doubled Alexandrite laser [22]
	852.0	Diode laser [23]
I ₂	514.5	Argon ion laser [24-31]
	532.0	Frequency-doubled Nd:YAG laser[32-34]
Ba	553.7	Dye laser [22]
Na*	589.0	Dye laser [35]
K	769.9	Ti: sapphire laser [36]
Rb	780.0	Alexandrite laser, Ti: sapphire laser [37-39]
Ce	894.4	Ti: sapphire laser [38]

*Sodium-seeded flame is used for elimination

Devlin and co-workers used iodine vapor absorption bands for eliminating an Ar-ion laser line ($\lambda = 514.5$ nm) in 1971 [24]. Two electronic vibrational-rotational absorption lines of iodine vapor were selected [40]. One is the transition from the 12th rotation level of the zeroth vibrational level of the ground electronic state ($X^1\Sigma_g^+$) to the 11th rotational level of the 43rd vibrational level of the ($B^3\Pi_u^+$) electronic excited state, i.e. 0-43 $P(12)$. The other is 0-43 $R(14)$ between the same electronic levels. For iodine vapor to work as a filter for the Rayleigh scattered argon-ion laser light, the laser must be single moded and the frequency of the single mode need to be accurately adjusted to 19429.82 cm^{-1} . Single moding of the laser is necessary because of the extreme narrow width of the iodine rotational line (250–300 MHz or about 0.01 cm^{-1}).

In the 1970s and 1980s, the iodine vapor filter was frequently used for low-frequency Raman or Brillouin scattering measurements, combined with a single-channel spectrometer such as a single/double monochromator or a Fabry-Pérot interferometer [28-34]. Wall and co-workers reported the use of an iodine vapor filter with multichannel detection [28-30]. They used a double monochromator converted to a polychromator and an intensified photodiode array for investigating surface enhanced Raman scattering from -60 to $+60\text{ cm}^{-1}$. The iodine vapor filter has not been used frequently after the 1990s, because the vibrational and rotational structure of the I_2 vapor absorption causes spiky artifacts appearing on the observed spectrum. The elimination of these artifacts was troublesome when the filter was used with a scanning spectrometer [25]. In 2009, Okajima and Hamaguchi revived the iodine vapor filter and developed a novel low-frequency Raman spectrometer by combining the filter with a multichannel detector [31]. Before this revival, the I_2 vapor filter has been used mainly for measurements of filtered Rayleigh scattering in flow field imaging [32, 33] and airborne lidar [34] instead of low-frequency Raman measurements.

The use of alkali metal vapor was reported in the 1990s [35-39]. Unlike iodine vapor, metal vapor has no vibrational and rotational structures in the absorption lines and does not give extra spiky artifacts in the spectra. Thus, intensity correction of the observed spectrum became quite easy. The only but most serious experimental problem in using metal vapor filters is the existence of strong resonance fluorescence at the absorption wavelength. Quenching gas such as Ar or N₂ should be added into the filter; otherwise the fluorescence interferes with the low-frequency Raman spectrum to a great extent. However, the quenching gas makes the absorption lines broader, so elimination bandwidth of the metal vapor filters is typically larger than a few cm⁻¹ [38].

I-5. Content of this thesis

The rest of this thesis is organized as follows. In Chapter II, I describe the multichannel low-frequency Raman spectrometer constructed in the present study. The working principle of this technique is mentioned in detail. In addition, the major components of the apparatus such as the iodine vapor filter, single-mode Ar-ion laser, and multichannel detector are described. The performance and advantages of the apparatus are also discussed in comparison with single-channel detection. In Chapter III, the application of the constructed low-frequency Raman system to the crystal polymorphs and melting process of 1,1'-binaphthyl is presented. The Raman spectra of the two crystal forms are compared especially for the spectral range below 200 cm⁻¹, which provide useful information about intermolecular interactions between 1,1'-binaphthyl molecules in the crystal structure. We also discuss the relationship between the Raman spectra of the two crystal forms and their crystal structures. Finally, I conclude my master work in Chapter IV and discuss the future perspective of low-frequency Raman spectroscopy in order to improve the spectral quality for better elucidation of low-frequency Raman spectra.

Chapter II

Construction of a Fast Multichannel

Low-Frequency Raman Spectrometer



II-1. Introduction

The low-frequency region ($<200\text{ cm}^{-1}$) of Raman spectra contains a wealth of information on intermolecular vibrations and lattice vibrations of molecular and ionic compounds in the condensed phase. In order to investigate the change of the crystal structure during the melting process, it is important to record a low-frequency Raman spectrum in a short measurement time ($<1\text{ sec}$). By using a multichannel detector such as a charge coupled device (CCD) camera, fast Raman measurements become possible. In the present study, we have constructed a fast multichannel Raman spectrometer, which can cover a wide spectral region ($-200\text{--}1100\text{ cm}^{-1}$). An absorption band of iodine vapor, having as narrow as 0.03 cm^{-1} bandwidth, is selected to eliminate gigantic Rayleigh scattering.

As mentioned in Chapter I, the iodine vapor had been used with a single-mode Ar-ion

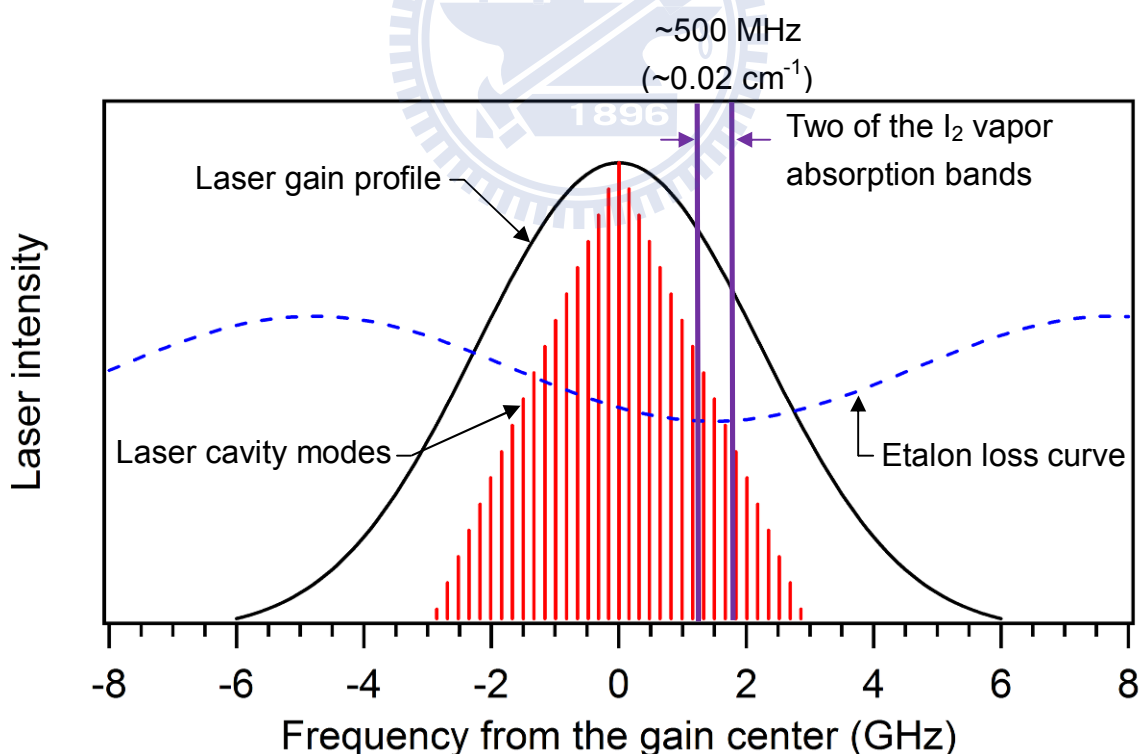


Figure II-1. Laser gain curve and cavity modes of an Ar-ion laser.

One of the absorption bands of iodine vapor is extremely close to the laser gain maximum (1.5 GHz higher).

laser in the 1970–80s for eliminating strong Rayleigh scattering [25-30]. Two of the iodine vapor absorption bands lie very close (1.5 GHz higher) to the gain maximum of an Ar-ion laser (figure II-1). These two absorption bands have a broader bandwidth (~500 MHz) than one laser cavity mode (40 MHz). Hence, The Rayleigh scattered light can be removed by this I₂ absorption band with high efficiency. Unfortunately, this excellent ability of I₂ vapor to get rid of Rayleigh scattering has rarely been used for Raman measurements because the superfluous artifacts caused by I₂-vapor absorption structure appear in the observed Raman spectra.

Not only the Argon ion laser but other single-mode laser can be combined with the I₂ vapor filter, because the iodine vapor has many vibronic transitions in the visible region [41, 42]. For the measurements of filtered Rayleigh scattering in flow field imaging [32, 33] or airborne lidar [34], a single longitudinal mode frequency-doubled Nd:YAG laser is combined with the iodine vapor filter (figure II-2). Also, a large number of the iodine vapor absorption bands are used as the spectral standard. Some of these absorption bands are used for stabilizing the frequency of various single-mode lasers; both gas lasers such as Ar-ion (514.5 nm) [43], Kr-ion (568.2, 530.9, 520.8 nm) [44], He-Ne (632.8 nm) laser [45-47], and solid-state lasers such as a frequency-doubled Nd:YAG (532.0 nm) [48, 49]. The versatility of the iodine vapor filter has been revealed above.

In what follows, the constructed low-frequency Raman spectrometer, which is composed of a single-mode Ar-ion laser, an iodine vapor filter, a polychromator and a CCD camera, is fully discussed. In addition, the advantages of the multichannel detection, especially high wavenumber reproducibility ($<1\text{ cm}^{-1}$) and short measurement time ($<1\text{ sec}$), are also shown.

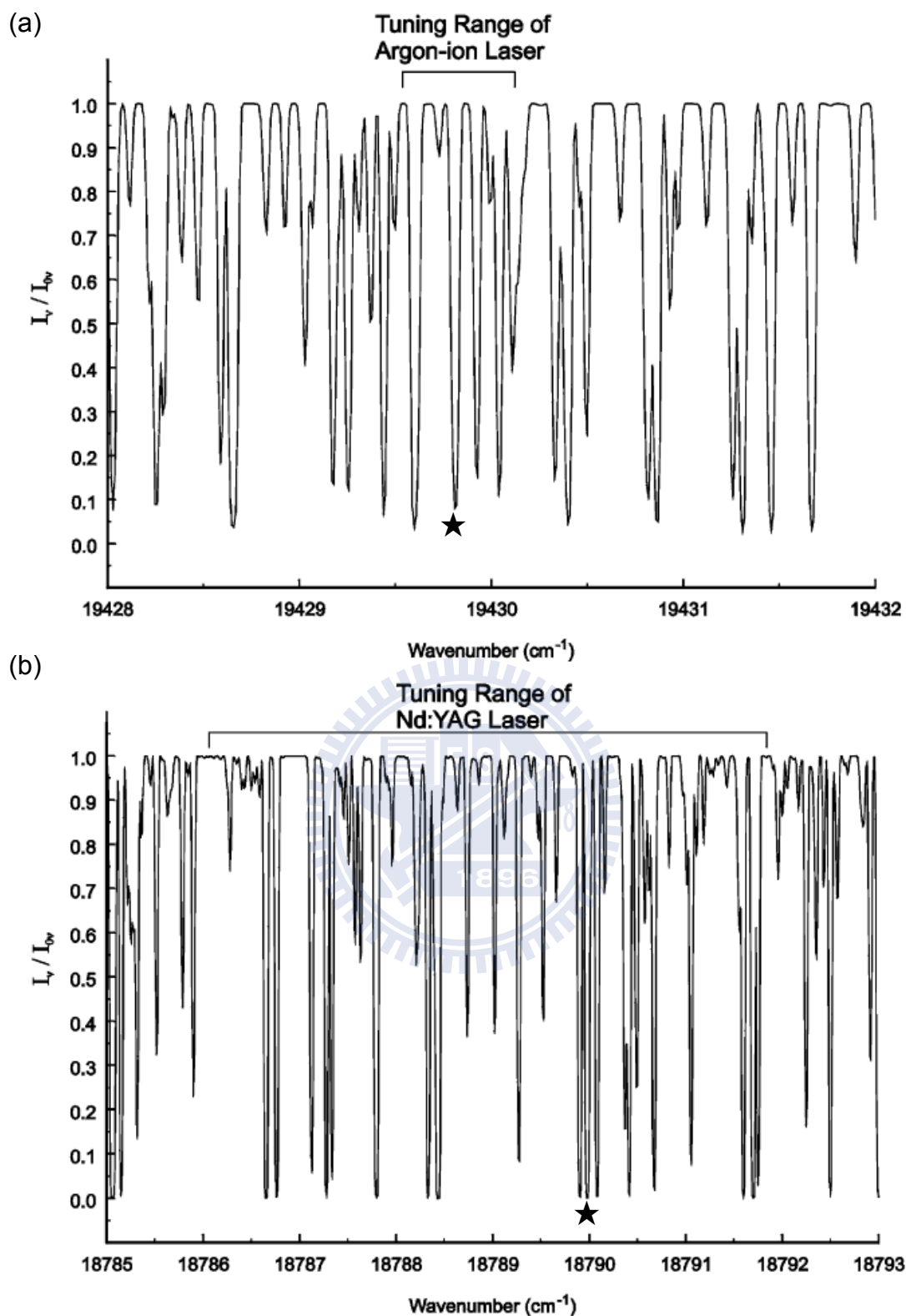


Figure II-2. Calculated absorption lines of I_2 in the visible frequency region accessible by (a) Ar-ion (514.5 nm), (b) Nd:YAG (532.0 nm) lasers.

(Taken from Gregory S. Elliott and Thomas J. Beutner, *Process in Aerospace Science* **35** 799 (1999).)

The 19429.82 cm^{-1} and 18789.90 cm^{-1} absorption lines (marked by stars) are used for laser line elimination of the single-mode Ar-ion laser and Nd:YAG laser, respectively.

II-2. Multichannel low-frequency Raman spectrometer using a single-mode Ar-ion laser (514.5 nm) and I₂ vapor filter

The fast multichannel low-frequency Raman system used in the present study was originally developed by Okajima and Hamaguchi [31] and subsequently constructed as a new setup at NCTU by us. In this section, the combination of a multichannel Raman spectrometer and an I₂ vapor filter is described. A single-mode Argon ion laser is used as the excitation source, which is the same as the previous low-frequency Raman studies [25-30] with an I₂ vapor filter. The advantages of this technique are also discussed.

II-2-1. Experimental setup

Iodine vapor filter

Figure II-3 shows the cylindrical cell (purchased from Sacher Lasertechnik) we used. It is made of glass with a diameter of 2.5 cm and a length of 10 cm, and contains iodine solids. Few milligrams of iodine are placed inside the cell and sealed at a high vacuum level ($<10^{-3}$ torr). The purity level of the natural elements used in manufacturing I₂ vapor cell is higher than 98%.

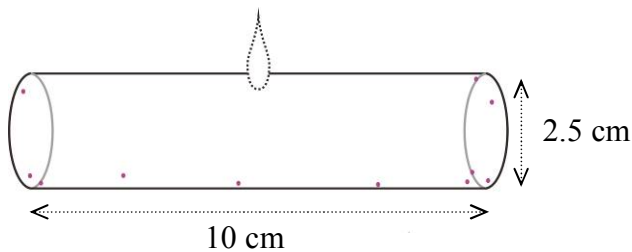


Figure II-3. Iodine vapor filter used in the present study.
(Purchased from Sacher Lasertechnik)

The iodine inside the cell is in the gas-solid equilibrium, and its vapor pressure depends on the temperature. Figure II-4 shows the pressure of iodine vapor under the gas–solid equilibrium estimated from the following equation [50].

$$\log (P) = 3.36429 - \left(\frac{1039.159}{T - 146.589} \right) \quad (311.8 \leq T \leq 456) \quad (\text{II-1})$$

where P is the vapor pressure of the I_2 vapor filter (bar), T is the temperature inside the cell (K). The vapor pressure increases almost exponentially with the temperature. A small fluctuation in the filter temperature causes a large change in the vapor pressure, which is proportional to the transmittance of the vapor filter. Therefore, the cell temperature should be highly stabilized during the experiment. In our I_2 vapor filter, we used a rubber heater, which wraps the whole glass cylinder in order to elevate the filter temperature (figure II-5). A chromel-alumel thermocouple placed between the rubber heater and filter is used to monitor the cell temperature. In each experiment, the cell temperature is kept at 95 °C and regulated within ± 1 °C during the measurement.

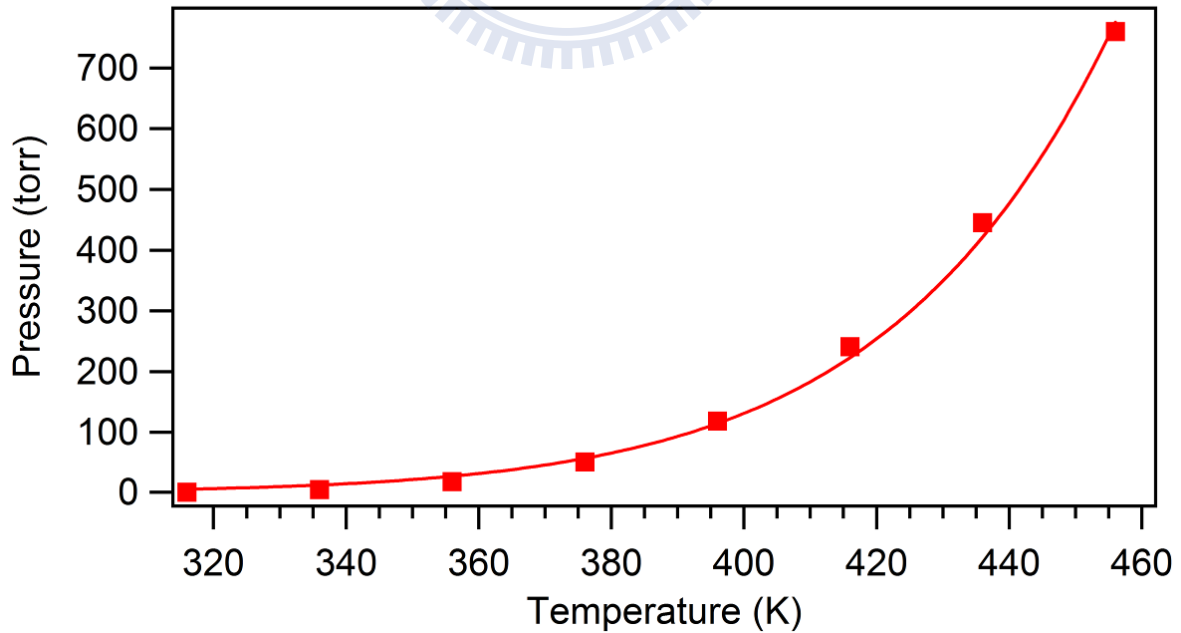


Figure II-4. Temperature dependent of iodine vapor pressure in the gas–solid equilibrium.

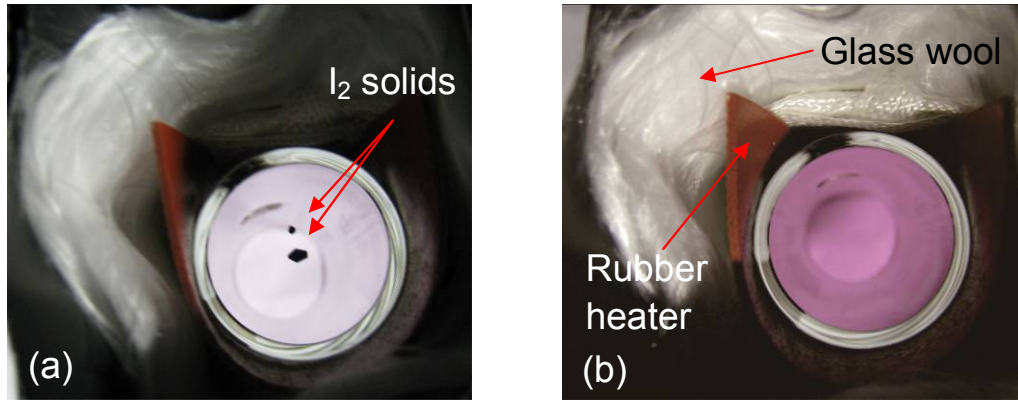


Figure II-5. Photographs of the I₂ vapor filter were taken at different filter temperatures
 (a) 24 °C (room temperature)
 (b) 95 °C

Single-mode Ar-ion laser

A water-cooled Ar-ion laser is used as the excitation source (Beam Lok 2060 with Z-Lok option, Spectra Physics). Figure II-6 shows a schematic diagram of this laser. An etalon consists solely of two partial reflecting surfaces with parallel alignment to each other. When it is inserted within a laser cavity, the partial reflectors create multiple, overlapping beams, which are directed out of the cavity by an intentional small tilt of the etalon with respect to the laser beam. Because of the “destructive interference” of the reflected beams at particular frequencies, almost no light actually comes out from the cavity. However, once the off-peak mode beams are reflected out of the cavity, the single-mode laser line is generated.

Because the cavity length of the laser is 1.1 meters, the mode spacing of each adjacent cavity modes is about 136 MHz. The full width at half maximum (FWHM) of the single-mode laser line is less than 40 MHz, which is much narrower than that of the iodine vapor absorption (~1 GHz). In order to fine tune the single-mode laser line to the I₂ vapor absorption band, the single cavity longitudinal mode located at the etalon loss minimum is selectively operated (figure II-1). By slightly changing the etalon temperature, the etalon loss minimum can be

tuned, and one longitudinal mode hops to next mode (mode-hopping). Also, the cavity length can be changed by slightly adjusting the piezoelectric (PZT) stage of the output coupler, a minor shift of the laser frequency (<100 MHz). In the experiments, both the etalon temperature and the PZT stage of the output coupler are controlled so that the observed Rayleigh scattering of the sample is maximally reduced.

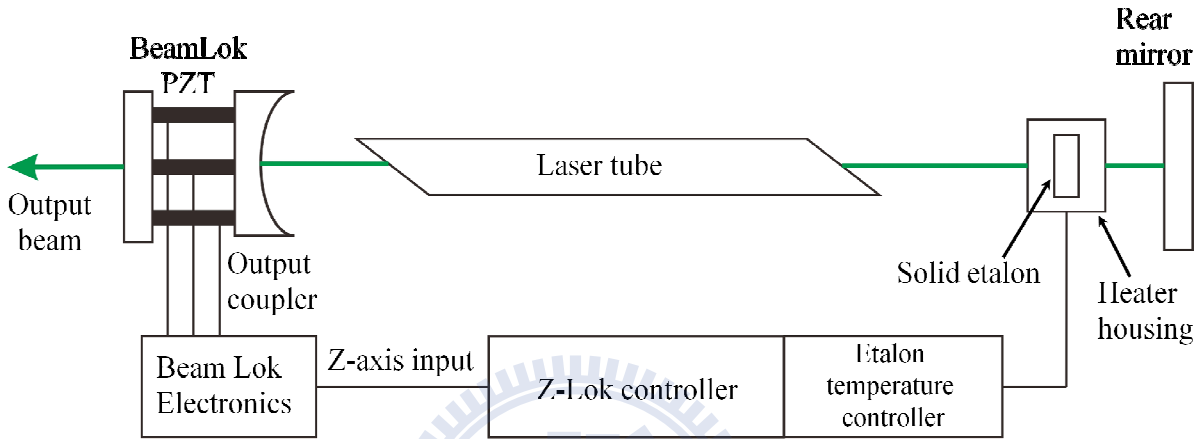


Figure II-6. Schematic diagram of a single longitudinal mode Ar-ion laser.

Apparatus

The constructed apparatus is schematically shown in figure II-7. The above-mentioned argon ion laser (514.5 nm) is used as the excitation source and the scattered light is collected at 90-degree by a camera lens ($f = 50$ mm, $f/1.2$, Nikon). The collimated light is passed through the I_2 vapor filter, which filters out most of the elastically scattered light. The transmittance is then focused onto the entrance slit of a polychromator ($f = 500$ mm, $f/6.5$, SP-2558, Princeton Instruments), and detected by a back-illuminated, deep-depletion, liquid-N₂ cooled CCD detector (Spec-10:100, Princeton Instruments) with 100×1340 pixels operating at -120 °C. The entrance slit width was typically set to 50 μ m. A 1200 grooves/mm grating was used to cover a wide spectral range (>1300 cm^{-1}) with a high spectral resolution of 2.7 cm^{-1} .

The white light from a tungsten lamp is monitored before and after each measurement to correct the intensity profile of observed Raman spectra. Furthermore, the transmittance of the white light spectrum can be used to remove the superfluous I_2 -vapor absorption structure. In order to introduce the white light into the filter with good position reproducibility, a flipper mirror and an aperture need to be placed in front of the I_2 vapor filter.

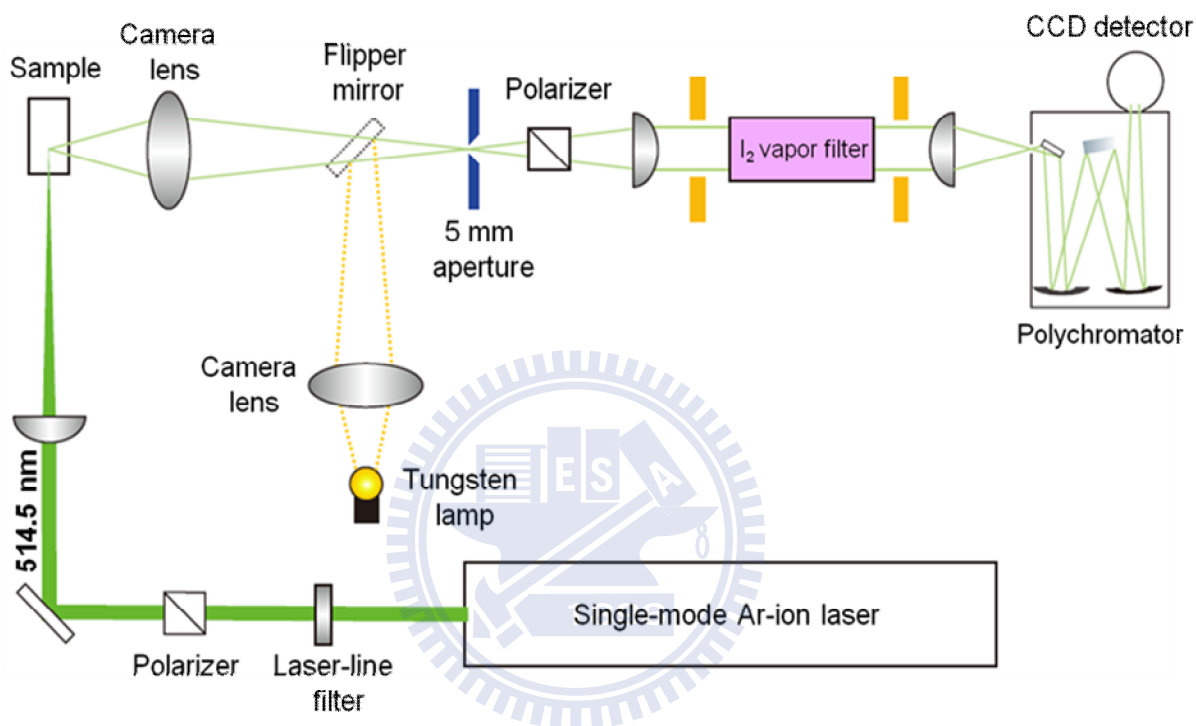


Figure II-7. Schematic diagram of the multichannel low-frequency Raman spectrometer.

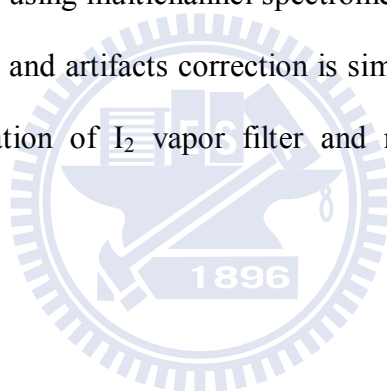
II-2-2. Results and Discussion

The intensity correction of the observed Raman spectra

To demonstrate how the intensity correction works, the Raman spectrum of carbon tetrachloride has been measured by using the apparatus in the present study. The observed and the intensity corrected Raman spectra are shown in figure II-8. The observed spectrum shows some superfluous artifacts due to I_2 -vapor absorption structure. The peak positions and

intensities of these artifacts precisely reproduce, indicating that they are not random noises but artifacts inherent to the I_2 vapor filter. These unwanted artifacts can be removed simply through dividing the observed spectrum by the white light spectrum.

It is noteworthy that the intensity and artifacts correction with scanning spectrometers is much more difficult than that with multichannel spectrometers because the wavenumber reproducibility of a scanning spectrometer is only about 1 cm^{-1} . The sharp spikes caused by I_2 vapor absorption appearing in the Raman spectrum and the white light spectrum require high spectral reproducibility for a rigorous correction. Thus, simultaneously detecting a wide spectral range ($>1300\text{ cm}^{-1}$) of spectrum without scanning the grating of the spectrometer is desirable [25]. In the case of using multichannel spectrometers, which have high wavenumber reproducibility, the intensity and artifacts correction is simply done as mentioned above. The real power of the combination of I_2 vapor filter and multichannel spectrometer is now demonstrated.



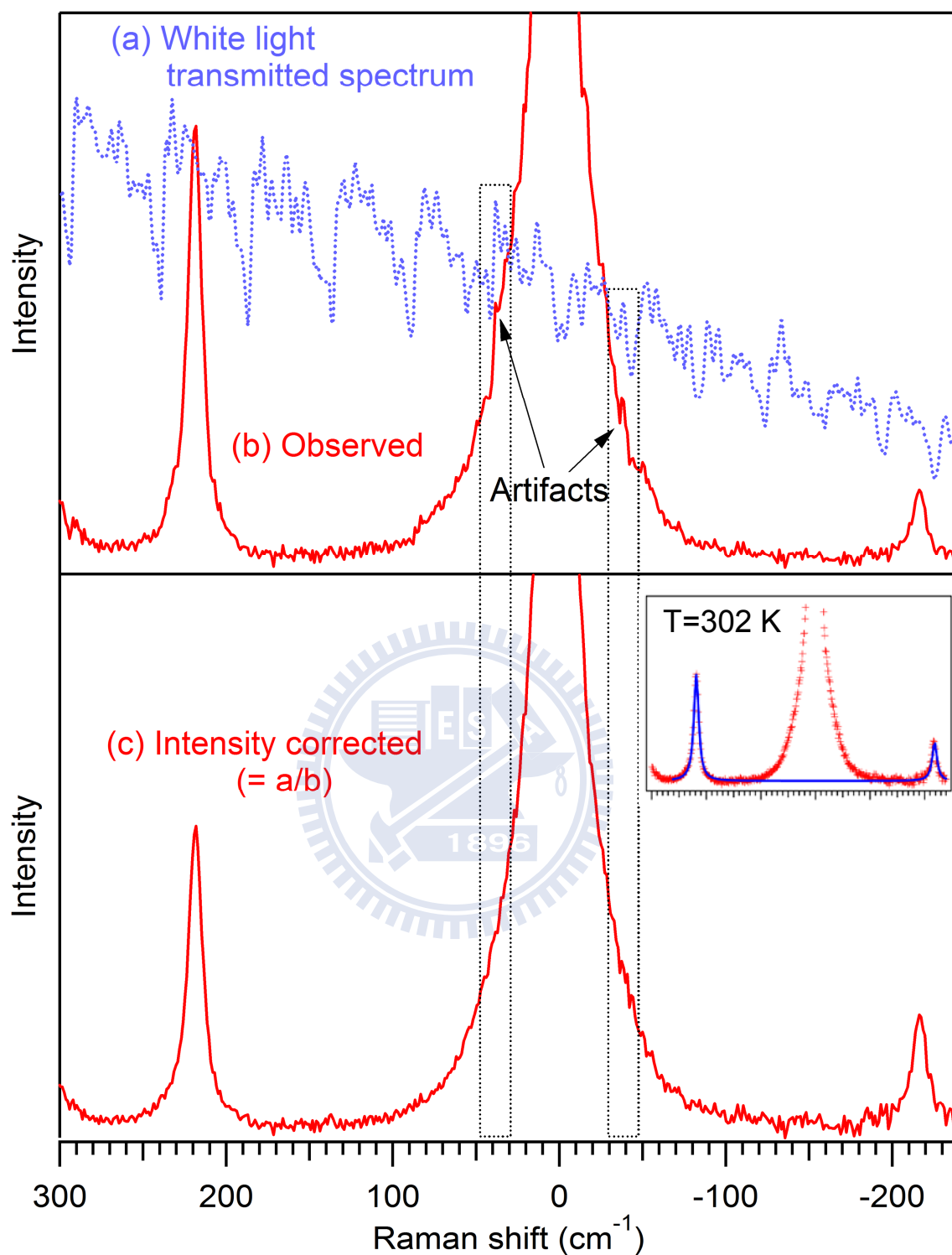


Figure II-8. Intensity correction of the Raman spectrum of CCl_4 .

- (a) White light transmitted through the I_2 vapor filter.
- (b) Observed Raman spectrum.
- (c) Corrected Raman spectrum (The inset is the fitting result for estimating the temperature, $T = 302 \text{ K}$).

Laser power at the sample point was 4.5 mW, the spectral resolution was 2.7 cm^{-1} , and the exposure time was (a) 50 sec and (b) 60 sec

It is possible to determine the sample temperature by measuring both the anti-Stokes and Stokes Raman spectra. The temperature at the sample point is estimated from the intensity ratio of the anti-Stokes and Stokes Raman lines using the equation [51] :

$$\frac{I(\text{anti-Stokes})}{I(\text{Stokes})} = \frac{(\tilde{\nu}_0 - \tilde{\nu}_m)^4}{(\tilde{\nu}_0 + \tilde{\nu}_m)^4} e^{-hc\tilde{\nu}_m/k_B T} \quad (\text{II-2})$$

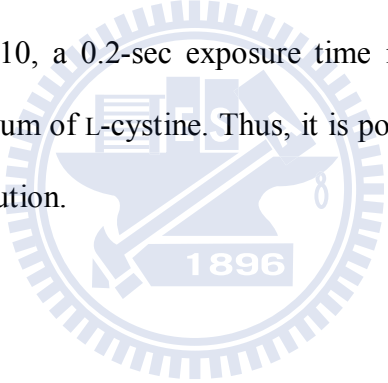
where $\tilde{\nu}_0$ is the wavenumber of the laser line, $\tilde{\nu}_m$ is the vibrational frequency of a band of the solvent or sample, h is Planck's constant, c is the speed of light, k_B is Boltzmann constant, and T is absolute temperature of the sample. This equation is based on the canonical distribution; hence it is not applicable when anti-Stokes lines are very weak. It should be noted that this equation is valid only for the spectra obtained under off-resonance conditions. The temperature of CCl_4 is estimated to be 302 K (the inset of figure II-8(c)), which is close to room temperature (298 K). Such temperature estimation is quite reliable if and only if multichannel detection is employed because both anti-Stokes and Stokes regions are measured simultaneously and the resulting anti-Stokes/Stokes intensity ratio is not affected by the intensity fluctuation of the laser.

Performance check: Low-frequency Raman measurement of L-cystine

In this section, we demonstrate the ability of our apparatus to measure low-frequency Raman spectra with a sufficiently exposure time by using L-cystine, which shows a Raman band at $\sim 10 \text{ cm}^{-1}$. The Raman spectrum of micro-crystalline powder L-cystine is shown in figure II-9. L-cystine was purchased from Wako Pure Chemical Industries (99.0% pure) and used without further purification. In order to obtain the corrected Raman spectrum of L-cystine, the intensity correction procedure mentioned previously was used. Due to high Rayleigh scattering elimination efficiency of the I_2 vapor filter, both the Stokes and anti-Stokes Raman spectra in the low-frequency region can be recorded with a small Rayleigh

gap (-5 to $+5\text{ cm}^{-1}$). The most intense Raman band of L-cystine at 498 cm^{-1} has nearly the same area intensity as that of the remaining Rayleigh scattering band at 0 cm^{-1} .

The constructed spectrometer enables us to record a wide spectral range (1300 cm^{-1}), including not only lattice vibrational modes but also intramolecular vibrational modes simultaneously. The low-frequency region of the Raman spectra of the L-cystine is shown in figure II-10. The $\pm 9.8\text{ cm}^{-1}$ band, which is usually used as a test of the performance of a low-frequency spectrometer, can be clearly observed. Because the present spectrometer employs a multichannel detection, it is not necessary to scan the spectrograph during the Raman measurement. Hence, the measurement time is, in principle, determined only by the exposure and read-out times of the CCD camera. The CCD read-out time in our case is 0.14 sec. As shown in figure II-10, a 0.2-sec exposure time is enough to measure a high S/N low-frequency Raman spectrum of L-cystine. Thus, it is possible to record a Raman spectrum with a sub-second time resolution.



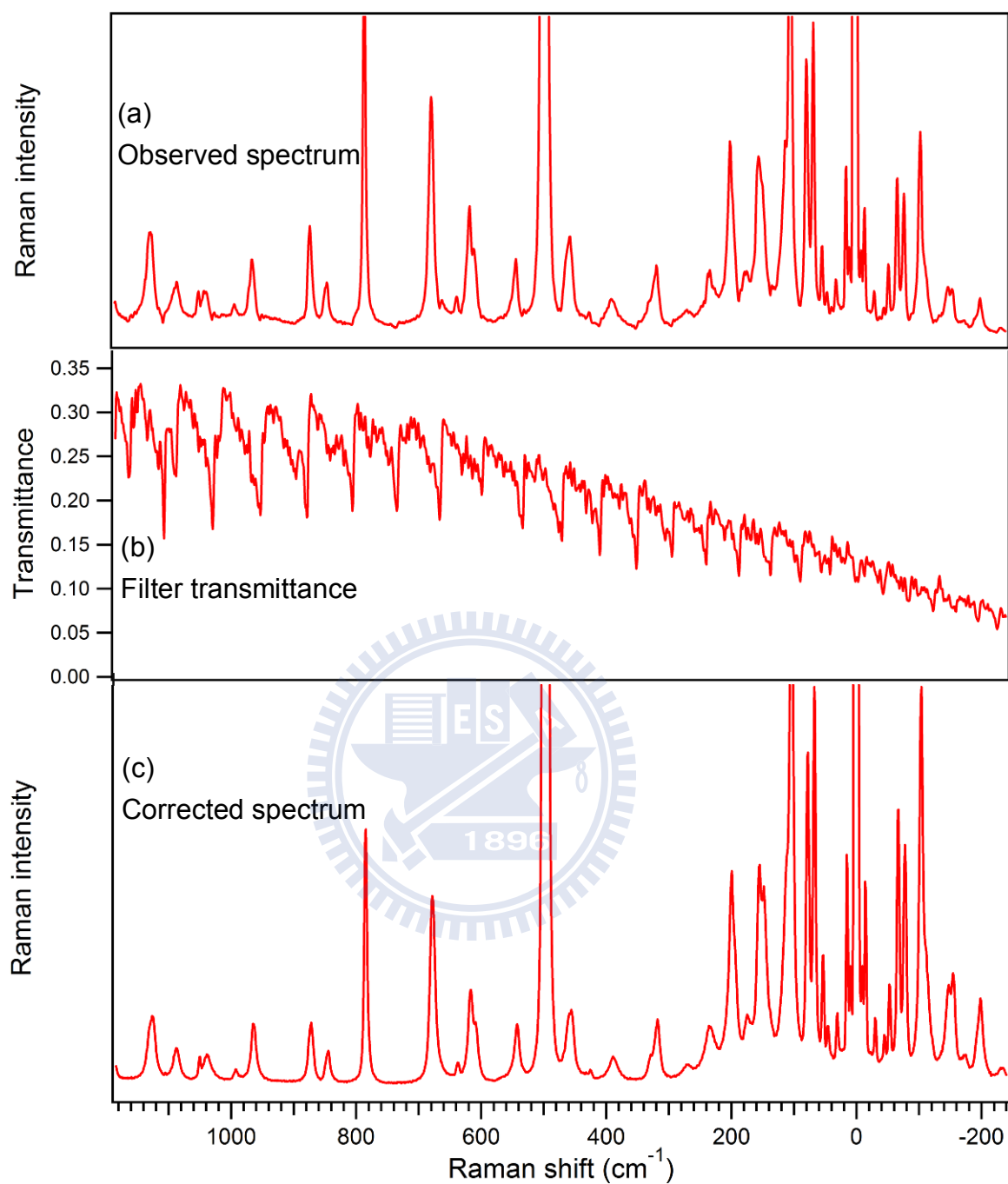


Figure II-9. Raman spectra of L-cystine.

(a) Observed Raman spectrum of L-cystine.

(b) Transmittance spectrum of I₂ vapor filter.

(c) Intensity corrected Raman spectrum of L-cystine (= a/b).

The measurement was done with 2.7 cm⁻¹ spectral resolution, 10 sec exposure, and 70 mW laser power.

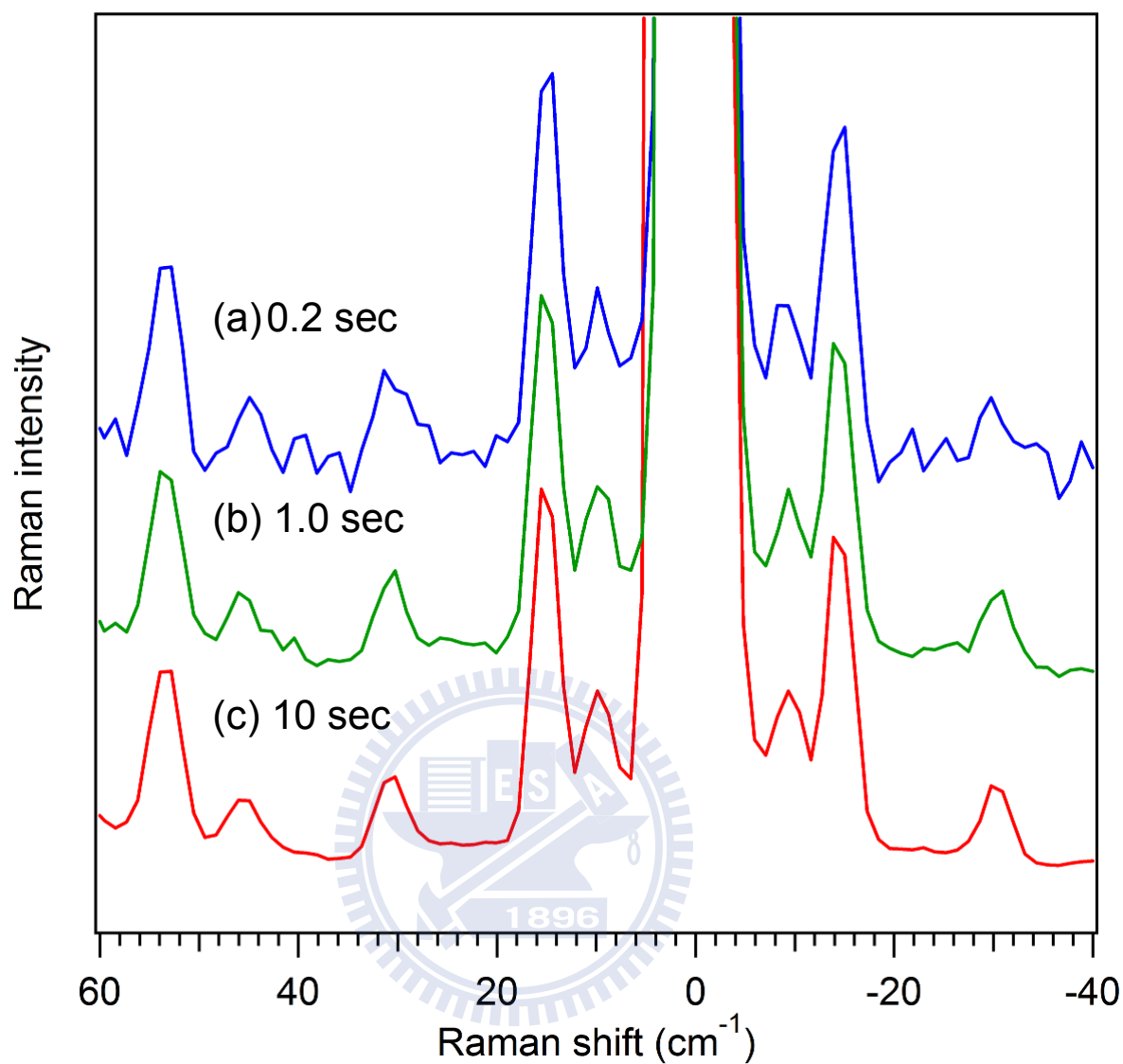


Figure II-10. L-cystine Raman spectra in the low-frequency region.

The measurement was done with different exposure times:

(a) 0.2 sec

(b) 1.0 sec

(c) 10 sec

Laser power was 70 mW, and the spectral resolution was 2.7 cm^{-1}

Comparison of I₂ vapor filter with commercial notch filters

The Raman spectra of L-cystine measured with three different filters are compared in figure II-11. As mentioned in Chapter I, typical notch filters having a broad Rayleigh rejection band ($>200\text{ cm}^{-1}$) can be seen in the blue line spectrum. Though the green line spectrum detects Raman bands below 100 cm^{-1} , the Raman bands at 67 and 78 cm^{-1} give incorrect relative intensity. A possible reason is that these two Raman bands were detected at the edge of the Rayleigh rejection bandwidth. The red line spectrum measured with the iodine vapor filter showing $\pm 9.8\text{ cm}^{-1}$ bands of L-cystine has already been discussed before. The excellent Rayleigh scattering elimination efficiency of the iodine vapor filter has been demonstrated here.

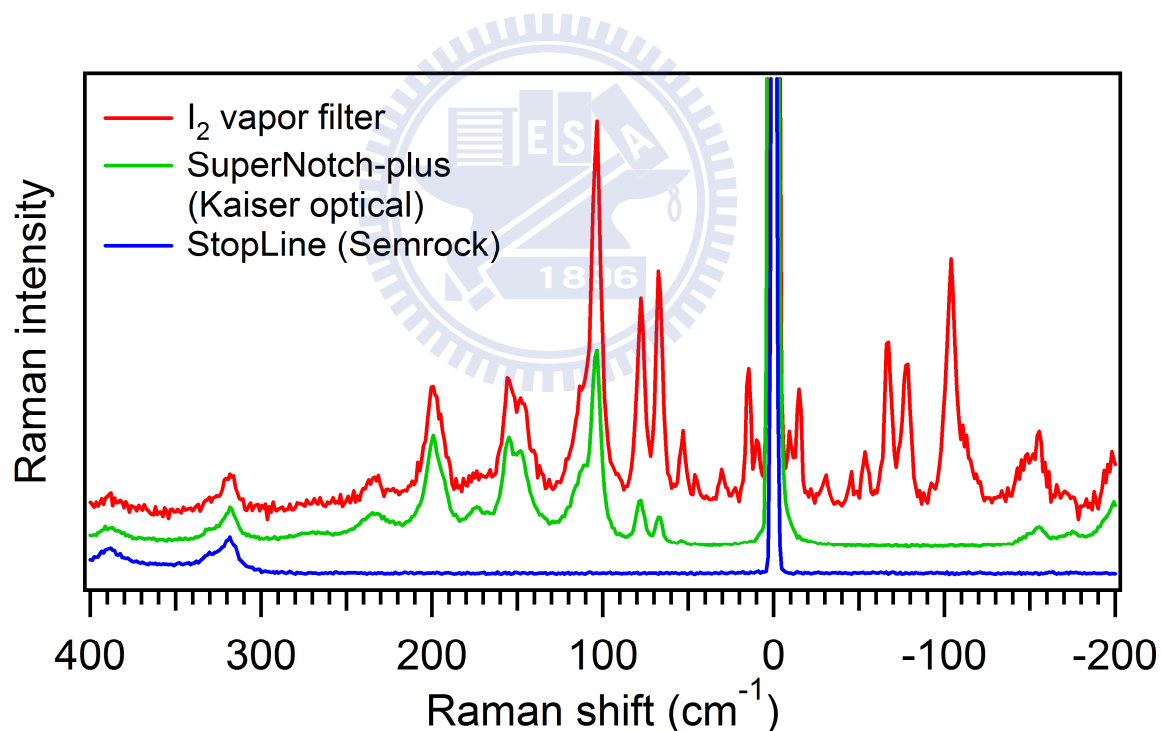


Figure II-11. Comparison of the Raman spectra of L-cystine measured with three different filters. Laser power at the sample point was 20 mW, the spectral resolution was 2.7 cm^{-1} , and the exposure time was 1 sec.

Artifacts due to the resonant fluorescence of iodine vapor

Although no fluorescence quencher is added into the I_2 vapor filter, resonant fluorescence of I_2 vapor makes no appreciable interference in the Raman spectrum of L-cystine as shown in figure II-9. This result contrasts with metal vapor filters such as potassium vapor-containing cell, in which resonant fluorescence is so strong that the addition of a quenching gas is necessary [36].

Fluorescence of iodine vapor is observed in the spectrum only when the strong laser light directly comes into the I_2 vapor filter. It occasionally happens when the laser light is reflected by the wall of a glass capillary and enters the collecting optics. Figure II-12(a) shows the Raman spectrum of L-cystine measured under such conditions. Extra bands other than the Raman bands of L-cystine are observed in this spectrum. The band at -13 cm^{-1} , which is close to the Rayleigh light, is due to spontaneous emission of the Ar-ion laser. Other bands ($212, 424, 637, \text{ and } 844\text{ cm}^{-1}$) result from the resonant fluorescence of the iodine vapor [52]. To reduce these annoying signals, the strong reflected laser light should be blocked. In a 90-degree scattering system, the removal of the reflected light is not so difficult. By placing an aperture in front of the I_2 vapor filter (figure II-7), the removal of the reflected light can be achieved easily. If a back or forward scattering geometry is employed for the measurement, quenching the fluorescence of the iodine vapor becomes much important. As a result, the fluorescence quencher may be required to be added to the filter similarly to the case of the metal vapor filters.

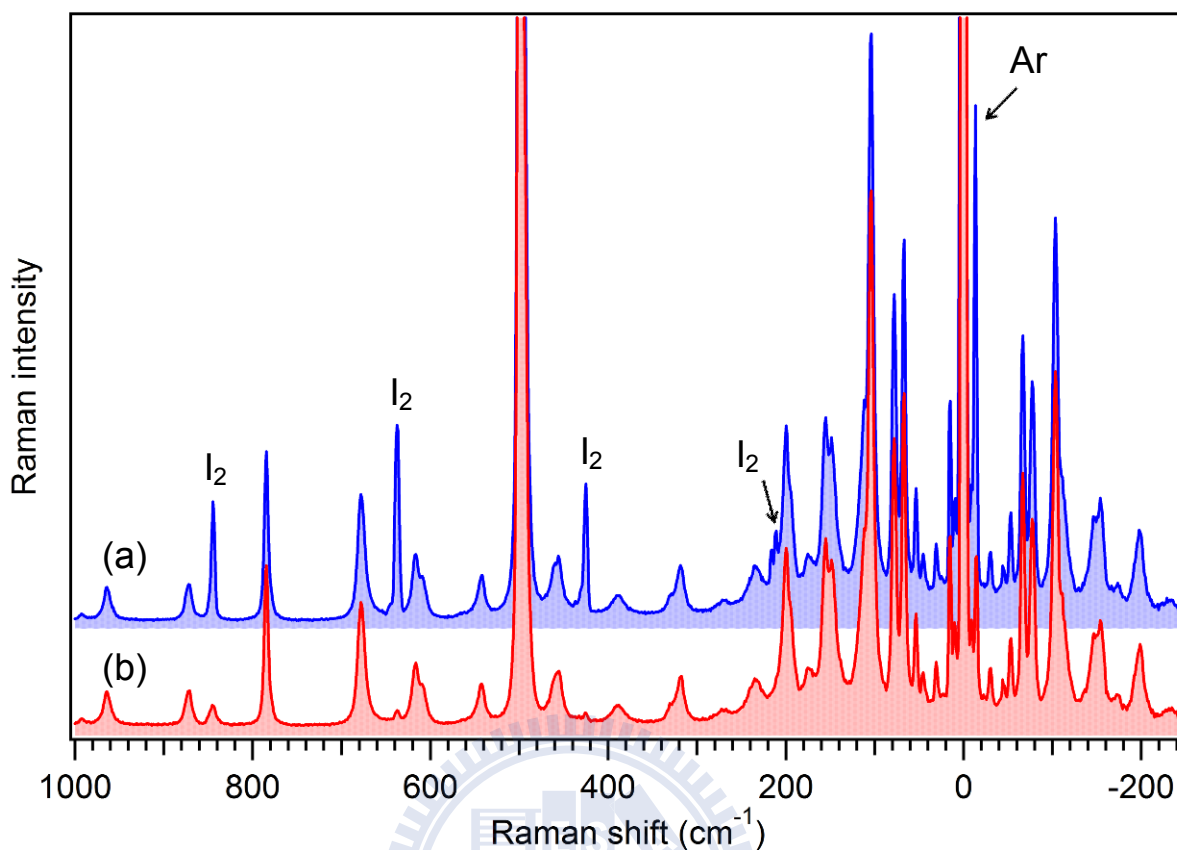


Figure II-12. Raman spectra of L-cystine obtained in the following two situations:
 (a) The laser light reflected by the glass capillary came into the I₂ vapor filter.
 (b) The reflected laser light was blocked by the 5 mm aperture.
 The mark “Ar” stands for spontaneous emission of the Ar-ion laser, “I₂” means the resonant fluorescence of I₂ vapor.

Raman spectral change caused by mode-hopping

During a long hour measurement, the selected laser cavity mode sometimes hops to another cavity mode (mode-hopping), because of the slight change of the etalon temperature. Once the mode-hopping occurs, the laser-line elimination of the iodine vapor filter become inefficient, and the observed spectrum drastically change in the low-frequency region. Figure II-13 shows the L-cystine Raman spectra using different cavity modes for measurement. When the mode-hopping occurs by only 0.3 GHz away from the optimum cavity mode, the observation of low-frequency Raman bands below 30 cm⁻¹ is found to be very difficult.

Hence, in order to avoid mode-hopping, it is crucial to keep the environmental temperature stable.

In particular, when the laser is operated for over five hour, it is necessary to confirm that the selected cavity mode exactly coincides with the iodine absorption band before starting the measurement. It can be easily confirmed by examining whether the Rayleigh scattering intensity still remains minimum or not.

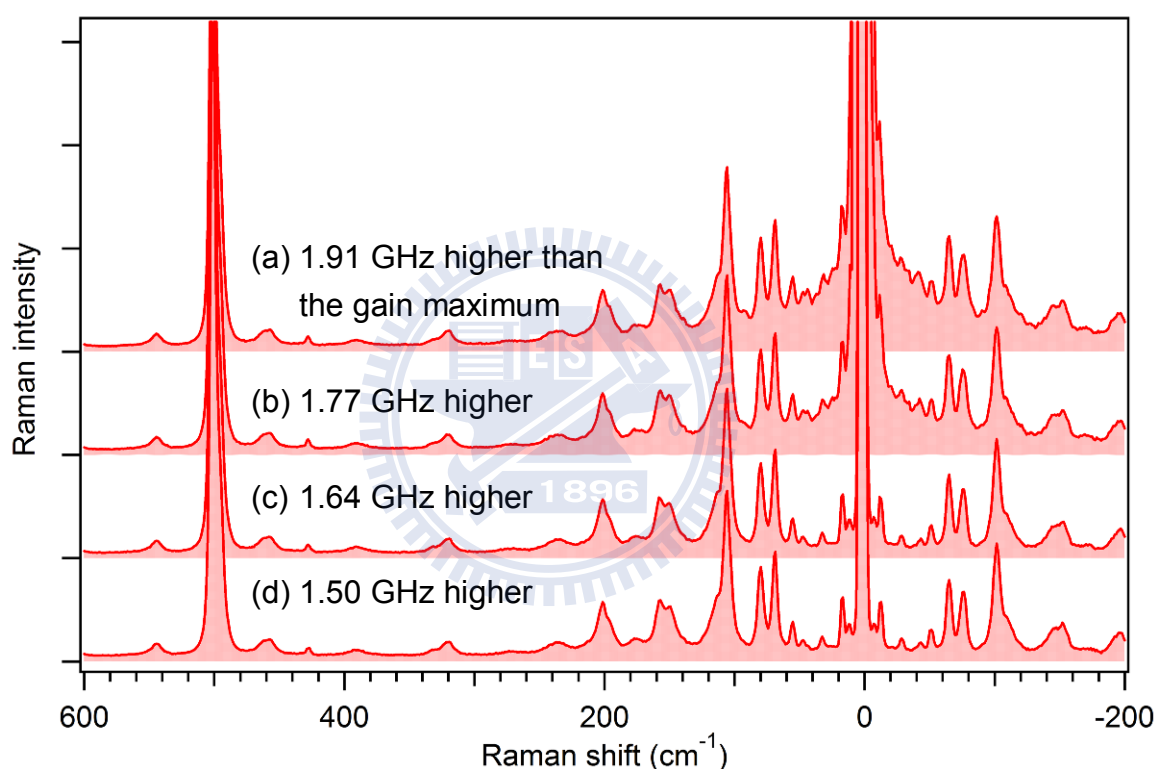


Figure II-13. Raman spectra of L-cystine measured by tuning the frequency of the single-mode Ar-ion laser.
(a) 1.91 GHz, (b) 1.77 GHz, (c) 1.64 GHz, and (d) 1.50 GHz higher than the laser gain maximum.

Chapter III

Real-Time Tracing of the Melting Process of the Two Distinct Polymorphs of Crystalline 1,1'-Binaphthyl



III-1. Introduction

1,1'-binaphthyl and its derivatives represent a special class of biaryl molecules. It is well-known for their application as chiral recognition receptors and chiral catalysts such as 2,2'-bis(diphenylphosphino)-1,1'-binaphthyl (BINAP) [53-55]. Biphenyl is the simplest biaryl molecule, in which two aromatic rings are linked via a C–C single bond. Its rotation barrier around the phenyl – phenyl bond in the gas phase was found to be ~1.4 kcal/mol [56]. 1,1'-binaphthyl, in which two naphthalene moieties are linked via a C–C single bond, has a substantially large increased rotation barrier of 23.5 kcal/mol (ΔG^\ddagger) [57]. The large rotation barrier is attributed mainly to the repulsion of the hydrogen atoms at the 8 and 8' positions. Besides, 1,1'-binaphthyl no longer possesses a plane of symmetry that biphenyl has in its perpendicular conformation. This fact allows the isolation of the optically active 1,1'-binaphthyl enantiomers. The dissymmetry of 1,1'-binaphthyl is molecular in nature, and enantiomeric interconversion is made possible simply by rotation about the interannular bond

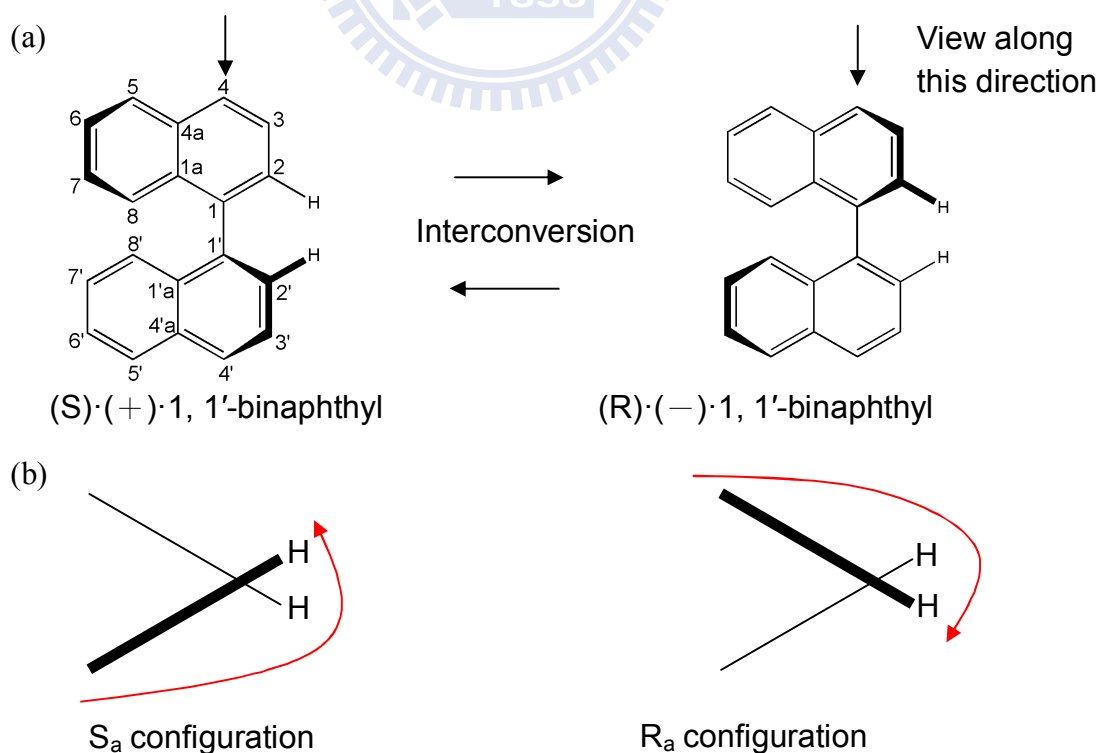


Figure III-1. Axial chirality of 1,1'-binaphthyl.

instead of by any bond-breaking process (figure III-1 (a)). The racemization half-life of the enantiomers was found to be 14.5 min at 50 °C. Chiral 1,1'-binaphthyl was discovered by Pincock et al. in 1971 [58]. He found that racemic 1,1'-binaphthyl underwent spontaneous resolution to generate the optically active R or S enantiomer when this compound crystallized from the melt.

The chiral 1,1'-binaphthyl molecule contains a chiral axis other than a chiral center. The enantiomers of axially chiral compounds are usually given the stereochemical labels R_a and S_a as shown in figure III-1 (b). The designations are based on the same Cahn–Ingold–Prelog priority rules used for tetrahedral stereocenters. In the crystalline state, 1,1'-binaphthyl is known to exist as at least two forms [59]: the cisoid configuration or lower melting point (148 °C) form and the transoid configuration or higher melting point (161 °C) form. Brown et al. [60] were the first to recognize the fundamental difference between the two forms. They found that the molecules of the lower melting point form take a cisoid configuration. X-ray diffraction [61] confirmed the dihedral angle θ to be 68.6° (figure III-2). Badar et al. [59] suggested, on the evidence of infrared spectroscopy, that the high melting point form adopts a transoid configuration, which was later confirmed by X-ray analysis [62] to have a dihedral angle of 103.1°. The cisoid form, whose structure was determined by Kerr and Robertson [61], consists of racemic monoclinic crystals (space group $C2/c$). The lattice unit ($Z = 4$) of this

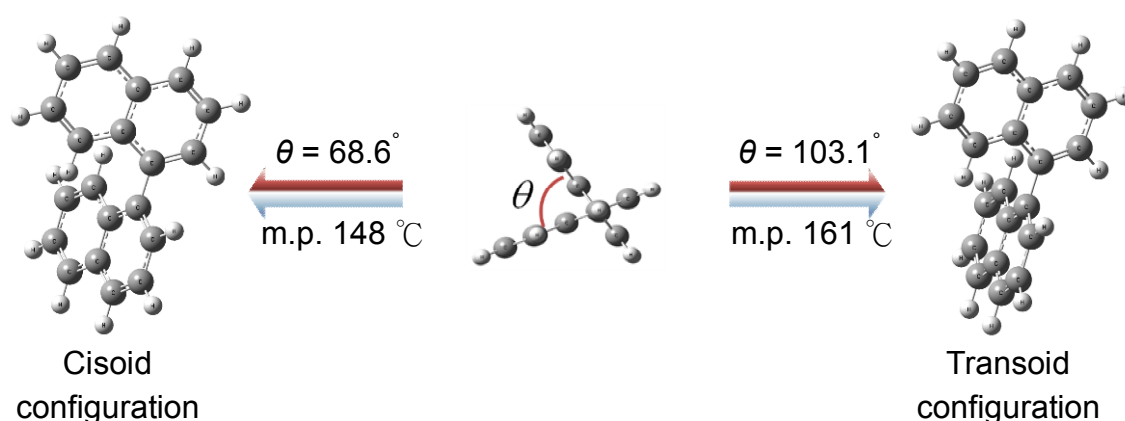


Figure III-2. Schematic diagram of the two crystal forms of 1,1'-binaphthyl.

achiral crystal is comprised of two R enantiomers and two S enantiomers. On the other hand, Kress et al. [62] reported the crystal structure of the transoid form as an optical active compound which belongs to the tetragonal system of space group $P4_212_1$ with either R or S enantiomer in a unit cell ($Z = 4$).

The molecular structural change of the ground and excited states of 1,1'-binaphthyl in the solution phase has also been studied by absorption spectroscopy [63, 64], fluorescence spectroscopy [65, 66], and Raman spectroscopy [66-68]. The molecule has also been the subject of many theoretical studies which have provided a wide range of estimates of the dihedral angle adopted by the 1,1'-binaphthyl molecule in its most stable conformations [69-75].

Raman spectroscopic studies on the two crystal forms of 1,1'-binaphthyl was first reported by Lacey et al [67] in 1986. However, their Raman spectra in the low-frequency region ($<150\text{ cm}^{-1}$) have not been reported yet. They showed a wealth of information about lattice vibrations of the crystal polymorphs. In addition, low-frequency Raman spectroscopy is sensitive to some intramolecular vibrations which have large amplitude, such as the C–C torsional motion of crystalline biphenyl [76]. Since the Raman intensity is proportional to the thermal average of the vibrational amplitude, large vibrational amplitudes will lead to large Raman intensities. Therefore, in the present study we applied the constructed low-frequency Raman spectrometer to 1,1'-binaphthyl, which has C–C torsional vibrations as well. The melting process of its two crystal forms has also been studied. We aim to understand the interplay between the intermolecular interactions and crystal structures of the two distinct polymorphs of 1,1'-binaphthyl (i.e., the cisoid and transoid forms) based on time-resolved low-frequency Raman spectra.

III-2. Experimental

Sample preparation

Solid 1,1'-binaphthyl of 98% purity, which turned out to be dominated by the cisoid form, was purchased from Tokyo Chemistry Industry Co., LTD. It contains unknown impurity which causes fluorescence appearing in the Raman spectrum with 514.5 nm excitation. We carried out crystallization with a procedure similar to that previously reported [58, 77, 78]. A schematic diagram of the crystallization procedure for obtaining two crystal forms of 1,1'-binaphthyl is shown in figure III-3. We placed a container with 500 mg of the sample in a bath of silicone oil and heated it to 180 °C. The melt was kept in this temperature for 20 min, ensuring that the whole sample had racemized completely. We then cooled the melt to 153 °C and allowed it to crystallize. In the first round (figure III-3 (a)), the transoid form was found

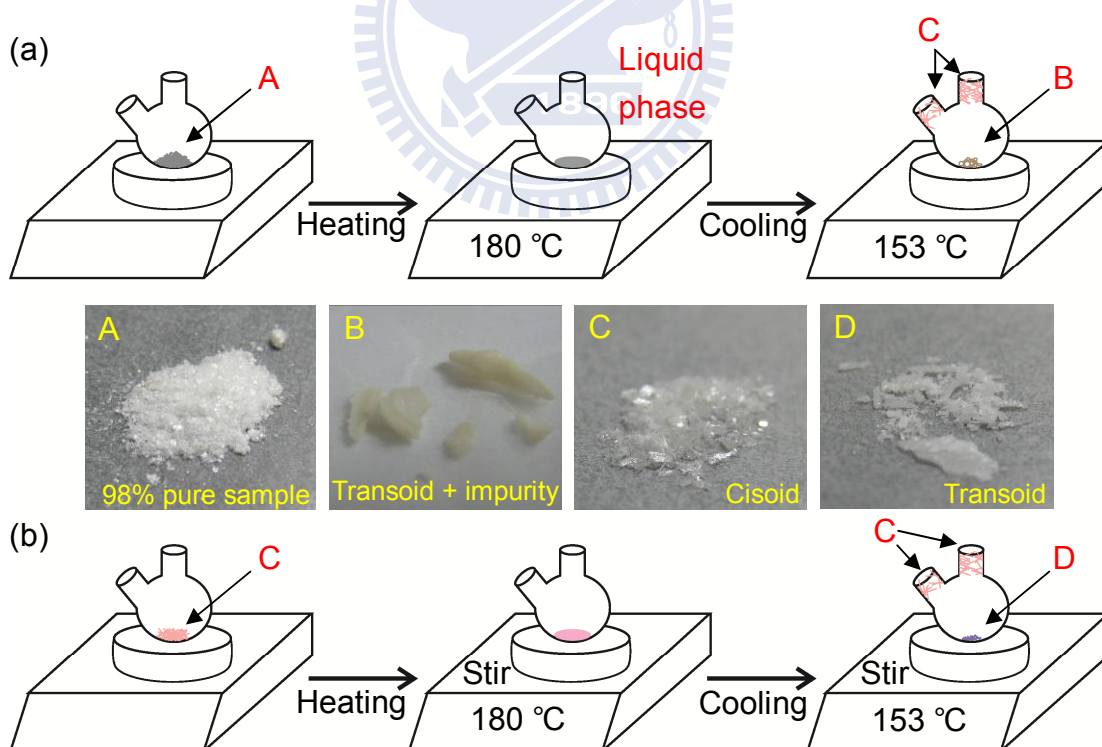


Figure III-3. Purification of commercially obtained 1,1'-binaphthyl and preparation of (a) cisoid form and (b) transoid form.

to be contaminated by the unknown impurity at the bottom of the container (marked as B in the figure). It was confirmed by our Raman apparatus that the product at the bottom gives stronger fluorescence compared with the sample before purification. Additionally, the pure cisoid form was observed as a result of the evaporation and recrystallization of 1,1'-binaphthyl from the vapor in the top part of the reactor (marked as C). This behavior is consistent with the vapor-solid process reported previously, where a polymorph transformation was observed in this compound [62]. In the second round (figure III-3 (b)), we used the pure cisoid form of 1,1'-binaphthyl obtained in the first round as the starting material to prepare the pure transoid form. The preparation method was the same as in the first round except for using a magnetic stir-bar in the container. Sainz-Díaz et al. reported that more transoid form formed if the reaction went under the condition of stirring [77]. They found that chiral symmetry breaking can be induced by stirring the melt as it crystallizes. For each crystal form, a small (~1 mm) piece of the pure crystal was sealed in a 1.2-mm glass capillary for rapid heating Raman measurement discussed below.

Heating apparatus

As shown in figure III-4, the hot air rework system (No.FR-802, HAKKO) with the power of 570 W was used for heating the samples from room temperature to the melting points rapidly. Its set temperature can be changed from 100 °C to 500 °C with an accuracy of ± 4 °C. In the case of 1,1'-binaphthyl, the melting points of its cisoid form and transoid form are 148 °C and 161 °C, respectively. The heating apparatus enables us to melt each crystalline form within 10 sec. Low-frequency



Figure III-4.
Photograph of the heating apparatus.

Raman spectral change during the melting was continuously measured every 0.2 sec.

III-3. Results

Raman spectra of the two distinct polymorphs of 1,1'-binaphthyl

The Raman spectra of two purified crystals were measured at room temperature as shown in figure III-5. For a comparison sake, the Raman spectrum of the commercially obtained 1,1'-binaphthyl was also recorded (the inset of figure) clearly seen from figure III-5

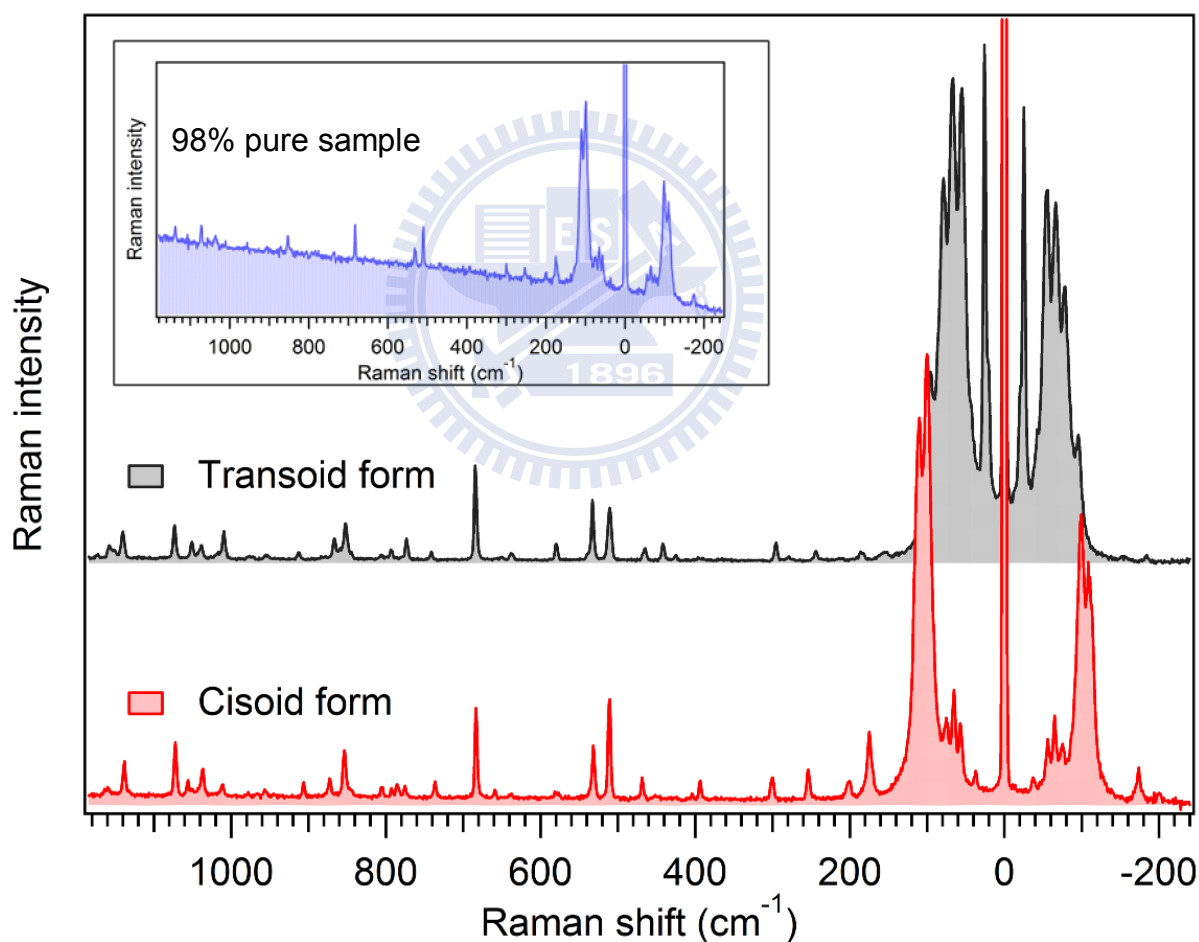


Figure III-5. Raman spectra of the two forms of crystalline 1,1'-binaphthyl.

The inset is the Raman spectrum of commercially obtained 1,1'-binaphthyl.

The spectra were measured with 30 mW laser power, 2.7 cm⁻¹ spectral resolution, and 0.2 sec exposure.

that strong fluorescence is observed for the commercial crystal with the spectral pattern being almost the same as the cisoid form, whereas no appreciable fluorescence is detected for both cisoid and transoid forms after purification. In addition, the spectral pattern in the region of $>150\text{ cm}^{-1}$ of the two crystal forms is consistent with the literature [67, 68]. The Raman intensities in this region appear to be similar. It should be noted that the bands in the higher-frequency region is much weaker in intensity than the bands in the low-frequency region $<150\text{ cm}^{-1}$, which indicates that these low-frequency vibrational motions accompany large polarizability changes than the intramolecular vibrations.

Figure III-6 shows the Raman spectra of the two polymorphs of crystalline 1,1'-binaphthyl in the -200 – $+200\text{ cm}^{-1}$ region. The Raman bands below 200 cm^{-1} both in Stokes and anti-Stokes sides have been recorded simultaneously. For the transoid form, the

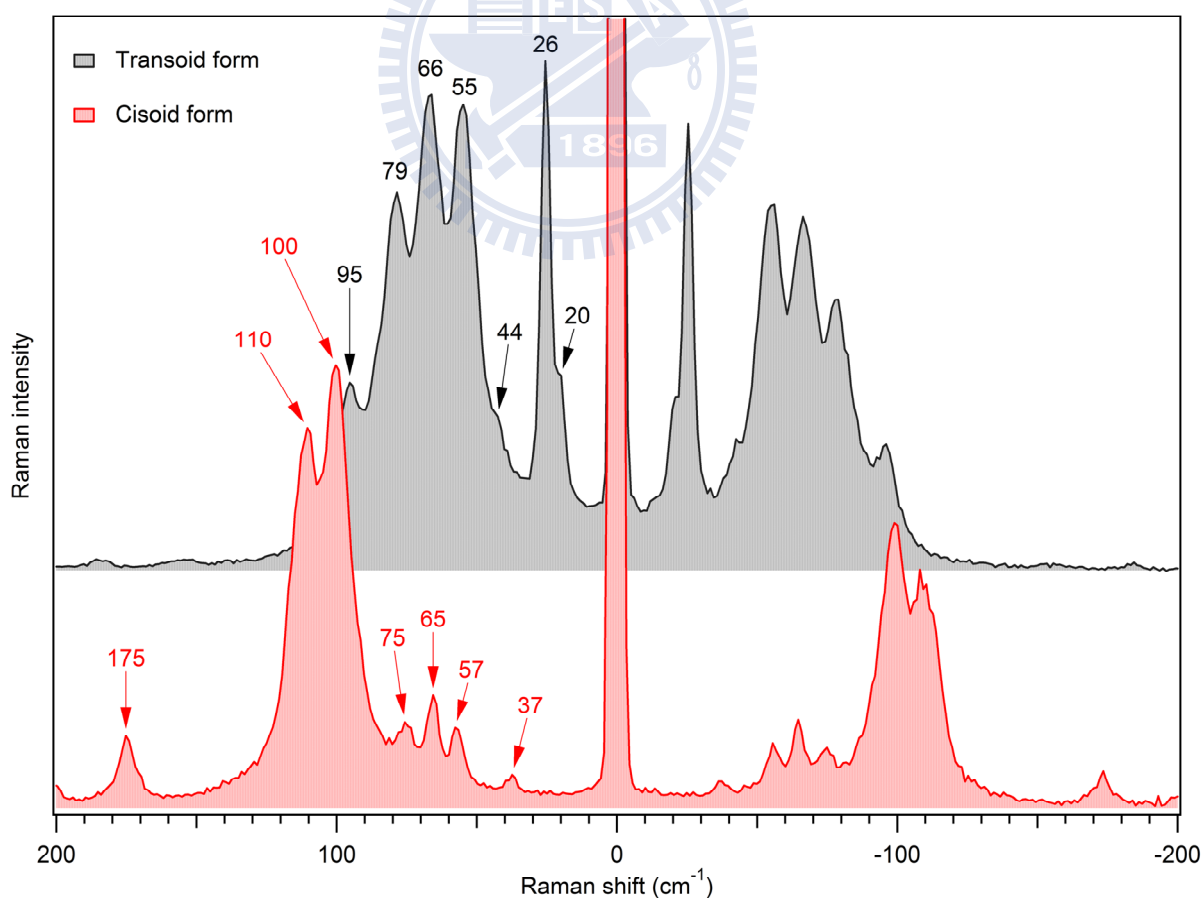


Figure III-6. Low-frequency Raman spectra of two crystalline 1,1'-binaphthyl.

$\pm 26\text{ cm}^{-1}$ bands, which are very close to the Rayleigh scattered peak, give the strongest intensity in the whole spectrum. On the other hand, the most intense band for the cisoid form is the doublet around 105 cm^{-1} , which may arise from a splitting of one band into two peaked at 100 and 110 cm^{-1} . The three Raman signals in the range of 46 to 90 cm^{-1} appearing in both crystal forms give similar peak positions. However, their band intensity in the transoid form is quite strong compared with that of the cisoid form. Such detailed information on the low-frequency Raman spectra of the crystal polymorphs of 1,1'-binaphthyl has been obtained for the first time.

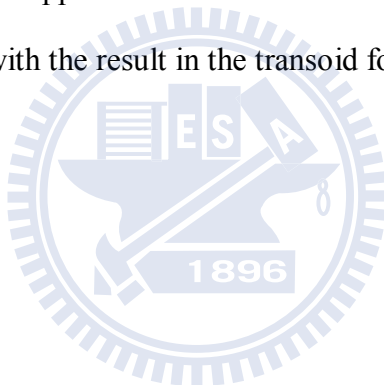
It is noteworthy that there are two small peak shoulders in the transoid form near 20 cm^{-1} and 44 cm^{-1} , which may be due to the lattice symmetry. These shoulders are so small that they can hardly be separately recorded. Thus, in order to investigate these shoulders appearing in the present data, high spectral resolution or polarized Raman measurements might be required in the future.

Raman spectral change during the rapid heating

Figure III-7 shows the low-frequency Raman spectra of a rapidly heated crystal of the transoid 1,1'-binaphthyl. Although each spectrum was recorded with as short as 0.2 sec exposure time, a high signal to noise ratio has been achieved. One of the intramolecular vibrations located at 295 cm^{-1} has been used for normalizing all the spectra. The spectral resolution for this measurement ($\sim 2.7\text{ cm}^{-1}$) is not high enough to separate the 20 cm^{-1} shoulder band from the band at 26 cm^{-1} . As the temperature goes up, the low-frequency Raman bands gradually lose their band shape and are hardly distinguishable 8 second after heating. Moreover, the central band at 0 cm^{-1} gets broadened and the S/N ratio of the spectra become lower at 7.6 sec . It may indicate that the liquid phase of 1,1'-binaphthyl appears at this moment. If we take a closer look at the two bands at 55 cm^{-1} and 66 cm^{-1} , they are

getting closer to each other as the temperature increases. However, the spectral pattern remains the same for the 79 cm^{-1} band before 7.4 sec. It is likely that these two bands are associated with quite similar vibrational motions and hence coupled to one another.

Tracing of the melting process of the cisoid form of 1,1'-binaphthyl has also been done and the result is shown in figure III-8. Normalization procedure was applied to all the spectra as mentioned before. Similarly to the previous experiment, the crystals melt at 6 sec judging from the 0 cm^{-1} band broadening and the reduced S/N ratio. We observe that the relative intensity of the two peaks at 100 and 110 cm^{-1} (strong doublet band) varies with increasing the temperature. It seems that the 100 cm^{-1} band intensity decreases upon melting. It is also clear that the 75 cm^{-1} band disappears soon while the bands at 57 and 65 cm^{-1} remain nearly unchanged. It is in contrast with the result in the transoid form.



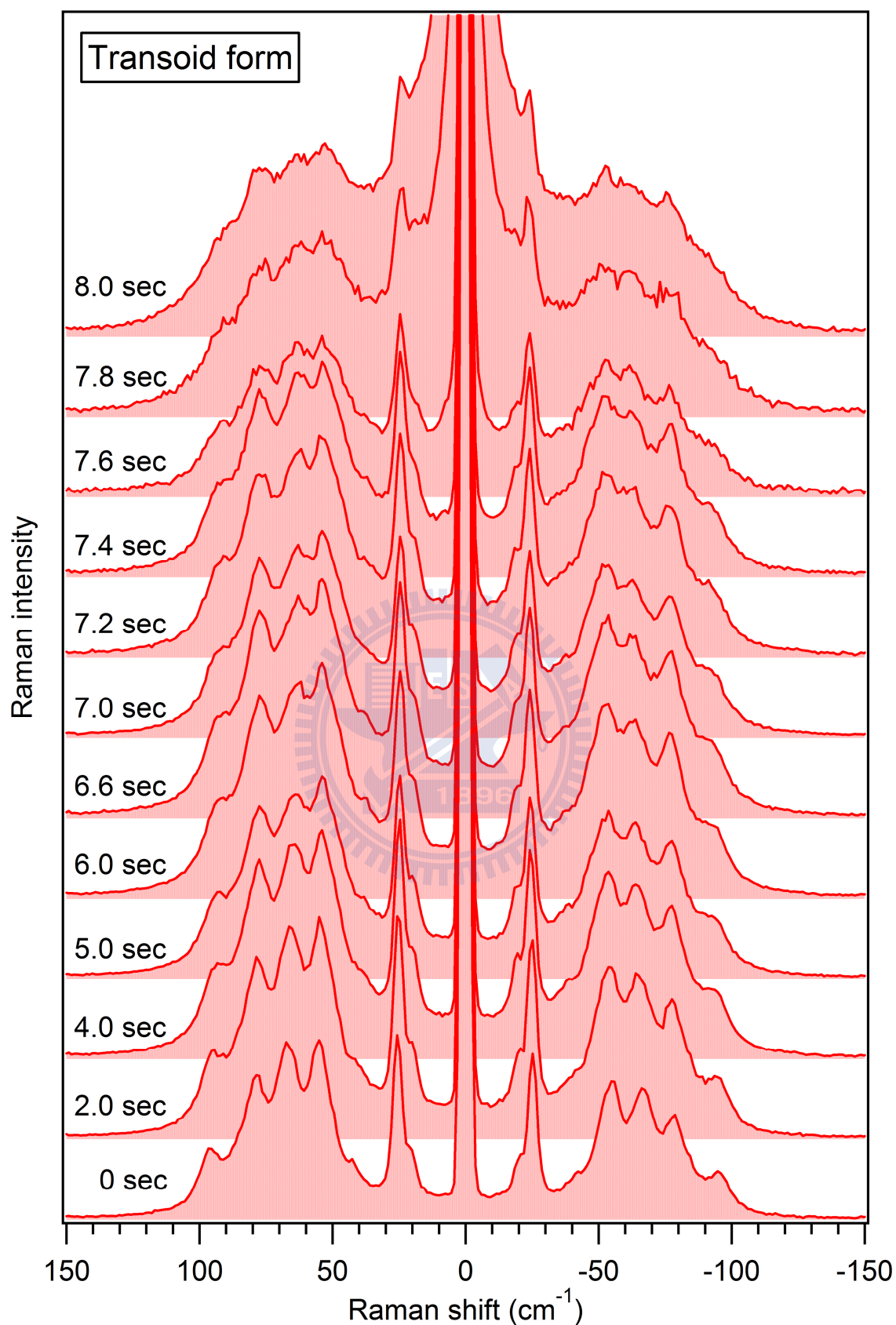


Figure III-7. Low-frequency Raman spectra of the transoid form with rapid heating. Each spectrum was measured with an exposure time of 0.2 sec, and the laser power and spectral resolution were 36 mW and 2.7 cm^{-1} , respectively.

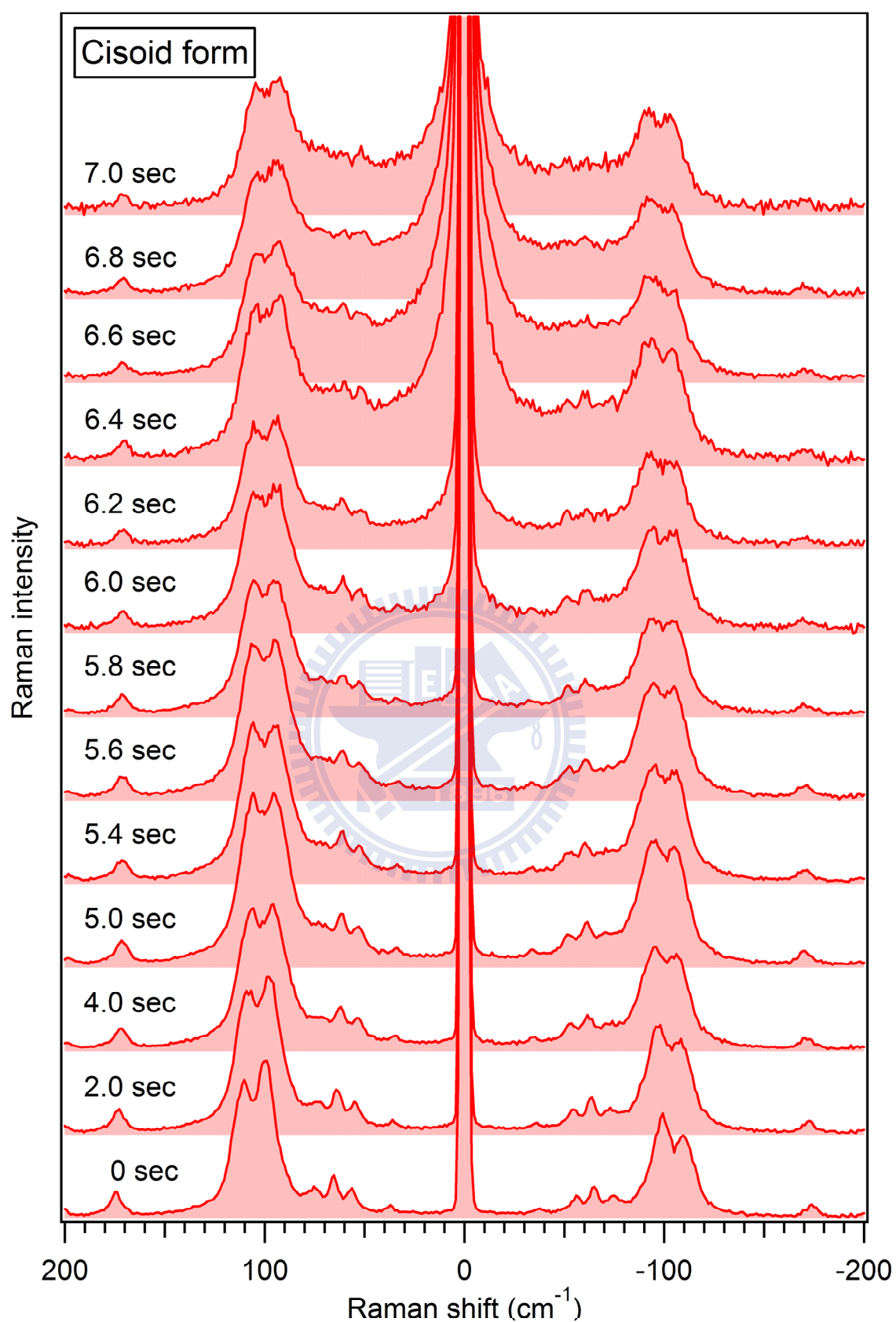


Figure III-8. Low-frequency Raman spectra of the cisoid form with rapid heating. Each spectrum was measured with an exposure time of 0.2 sec, and the laser power and spectral resolution were 31 mW and 2.7 cm^{-1} , respectively.

III-4. Fitting analysis

Although there are a number of low-frequency Raman bands below 200 cm^{-1} in both crystal forms of 1,1'-binaphthyl, both the Stokes and anti-Stokes sides can be fitted well assuming Lorentzian band shapes. The sample temperature as well as the peak position of each low-frequency Raman band was estimated by means of the fitting. Details of the procedure are described below.

Lorentz function was used for fitting each low-frequency band including the two peak shoulders for the transoid form. Since the Stokes and anti-Stokes sides of each Raman band have the same peak position and band shape, the Lorentz function used for the fitting should be symmetrical with respect to the 0 cm^{-1} Raman shift, like the following function.

$$\frac{A_i}{(\tilde{\nu} - \tilde{\nu}_i)^2 + \Delta_i^2} + \frac{A_i}{(\tilde{\nu} + \tilde{\nu}_i)^2 + \Delta_i^2} \quad (\text{III-1})$$

where $\tilde{\nu}$ is the Raman shift, $\tilde{\nu}_i$ is the peak position, A_i is the band intensity, and Δ_i is the bandwidth. This function has two peak positions at $+\tilde{\nu}_i$ (Stokes side) and $-\tilde{\nu}_i$ (anti-Stokes side). If $\tilde{\nu}_i$ is zero, equation III-1 reduces to one single Lorentz function located at 0 cm^{-1} , representing the Rayleigh scattering.

The intensities of the Stokes and anti-Stokes bands are not the same, hence an important factor must be included in equation III-1. As we mentioned in Chapter II, the anti-Stokes/Stokes intensity ratio is related to the Boltzmann distribution in the vibrational energy levels (equation II-2). Considering the Stokes and anti-Stokes intensity difference results from the thermal effect, it can be compensated by multiplying the symmetrized Lorentz function (equation III-1) and the Bose-Einstein factor ($n(\tilde{\nu})$) [79] :

$$n(\tilde{\nu}) = \left(1 + \exp\left[-\frac{ch\tilde{\nu}}{k_B T}\right]\right)^{-1} \quad (\text{III-2})$$

Where c is the light velocity, h is the Planck's constant, k_B is the Boltzmann constant, and T is the sample temperature. Note that the extra fitting parameter required is only the temperature (T). In the fitting, the temperature parameter of all the low-frequency Raman bands is assumed to be the same.

Table III-1 summarizes the fitting parameters. Symmetrized Lorentz function convoluted with the Bose-Einstein factor was applied to fit the seven low-frequency Raman bands of the cisoid form as well as those of the transoid form in both Stokes and anti-Stokes sides. Twenty-three independent parameters are determined simultaneously for each fitting.

Table III-1.	
Baseline	y_0
Peak position	$\tilde{\nu}_i$ ($i = 1-7$)
Bandwidth	Δ_i ($i = 1-7$)
Intensity	A_i ($i = 1-7$)
Temperature	T

The fitted results of the Raman spectra of the two crystalline forms of 1,1'-binaphthyl are shown in figures III-9 and III-10, they were done under the unnormalized condition. Whether the spectra are normalized or not would not affect the determination of the sample temperature because it is obtained from the relative intensities of the Stokes and anti-Stokes bands rather than from their absolute intensities. The fitting was done in the spectral region below 200 cm^{-1} except for the Rayleigh gap region (-15 – $+15 \text{ cm}^{-1}$), but was not possible for the spectra recorded after 7 sec in both cases of the two crystal forms. Judging from the results as shown in figures III-9 and III-10, the low-frequency Raman bands were fitted well in both crystal forms before 7 sec. Though we observe that the Raman band intensity dropped a lot at 6 sec for the cisoid form, the line intensity as well as line shape of these low-frequency bands still can be reproduced fairly well by the fitting. In addition, it is noteworthy that the

shoulder peaks at 20 and 44 cm^{-1} in the Raman spectra of the transoid form can also be fitted well.

Based on these high quality fitting results, the sample temperature can be estimated to a high accuracy. Moreover, the peak position of each low-frequency Raman band has also been determined by the fitting. Thus, the sample temperature change and peak position shift of the low-frequency Raman bands will be the main topic in the following sections. And the spectral differences between the cisoid and transoid forms during the heating and their possible explanations will be discussed as well.



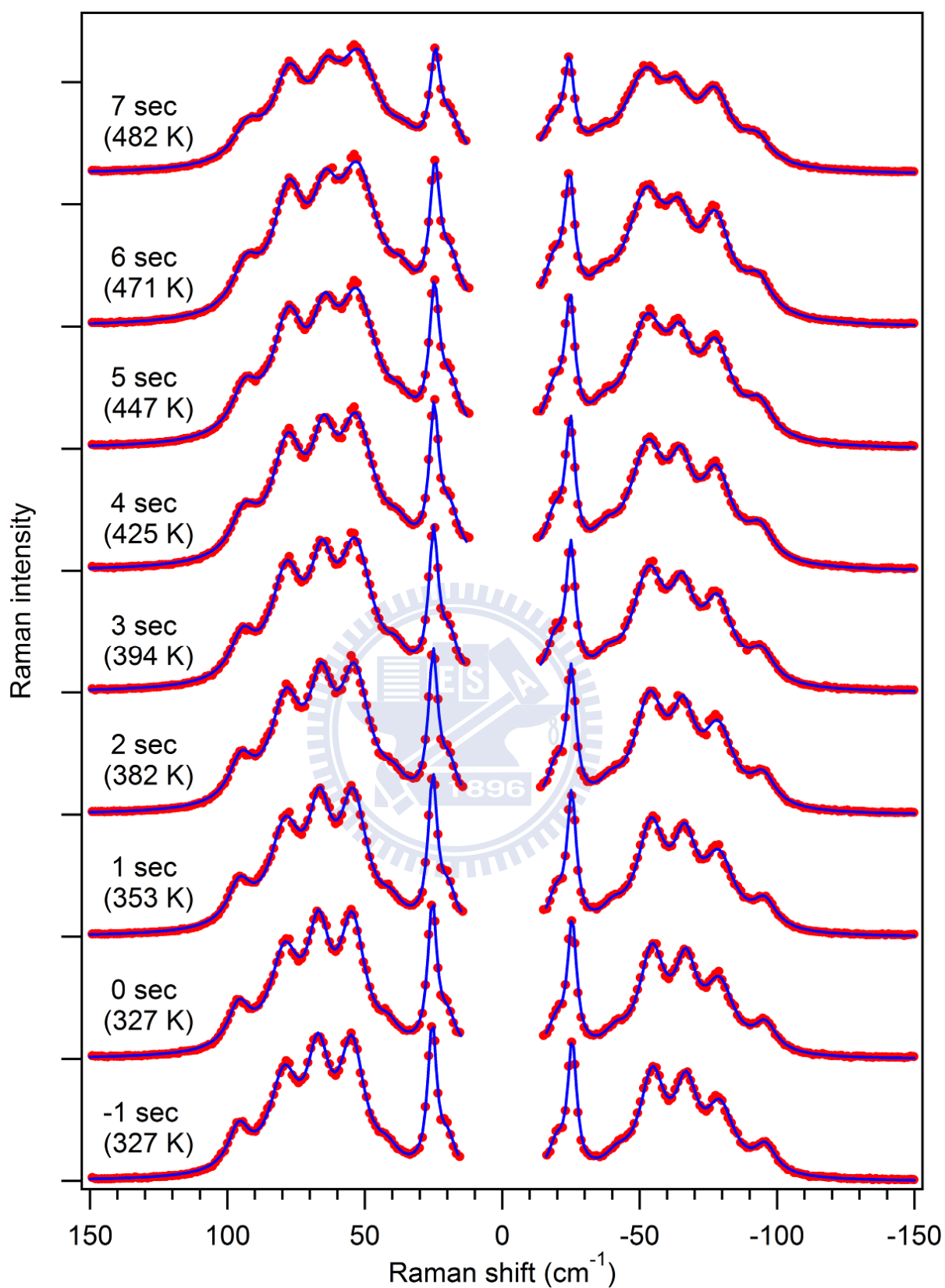


Figure III-9. Experimental data (red closed circles) of the transoid form and their fitted results (blue solid lines).

The sample temperature at each time was estimated from the fitting.

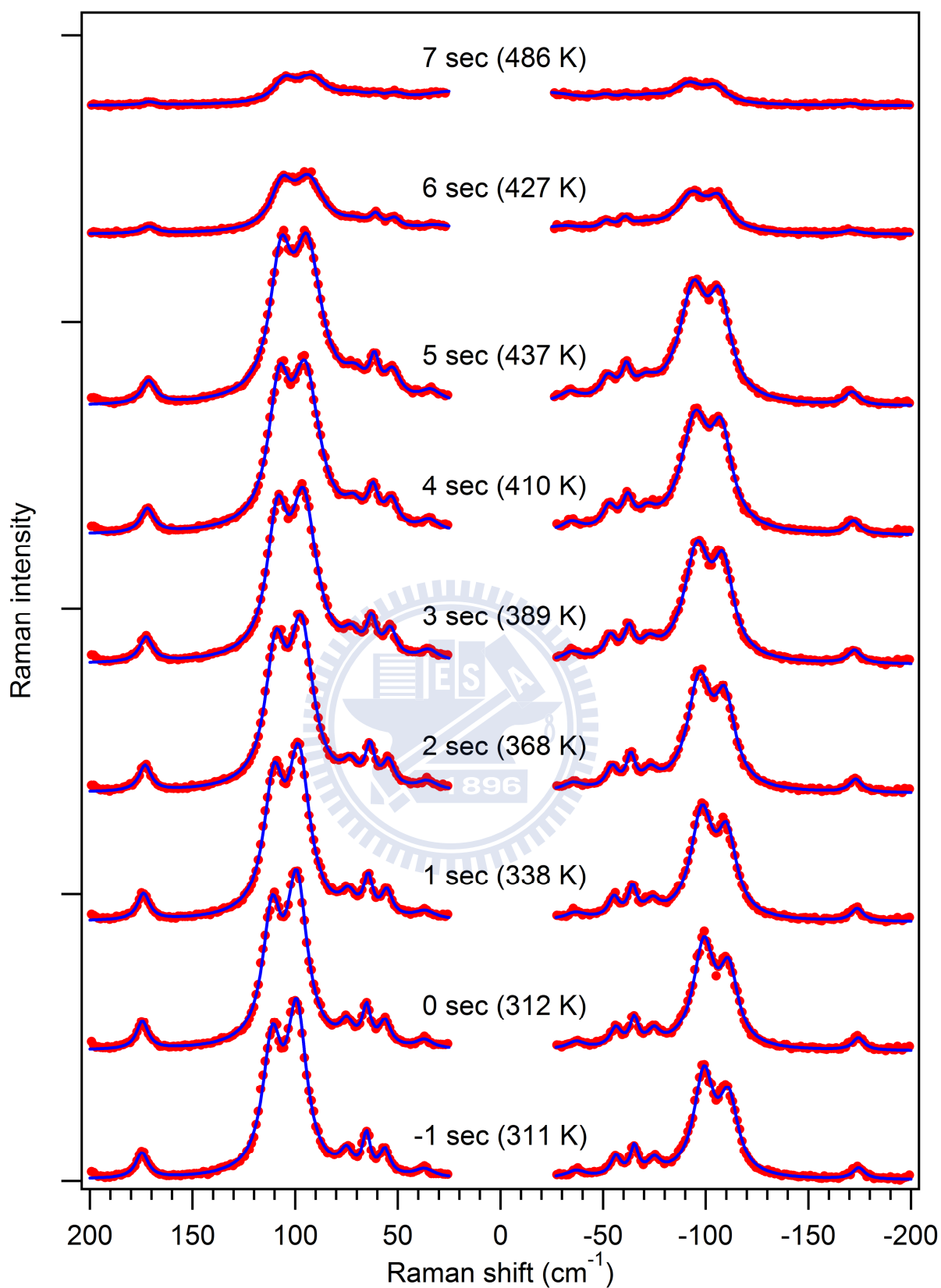


Figure III-10. Experimental data (red closed circles) of the cisoid form and their fitted results (blue solid lines).
The sample temperature at each time was estimated from the fitting.

III-5. Discussion: Temperature change during the melting

Temperature change of the cisoid form upon heating

How the temperature changes with the heating time in the case of the cisoid conformer of 1,1'-binaphthyl is shown in Figure III-11. Each temperature was estimated from the Raman spectra shown in figure III-8. The estimated temperature before starting heating (<0 sec) is about 315 K with a fluctuation of ± 6 K. It is 17 °C higher than the room temperature (298 K) because of the high laser power used. After the heating starts, the sample temperature increases rapidly to over 486 K in 7 sec. By differential scanning calorimetry (DSC) measurement, the melting point of the crystalline 1,1'-binaphthyl can be obtained (figure

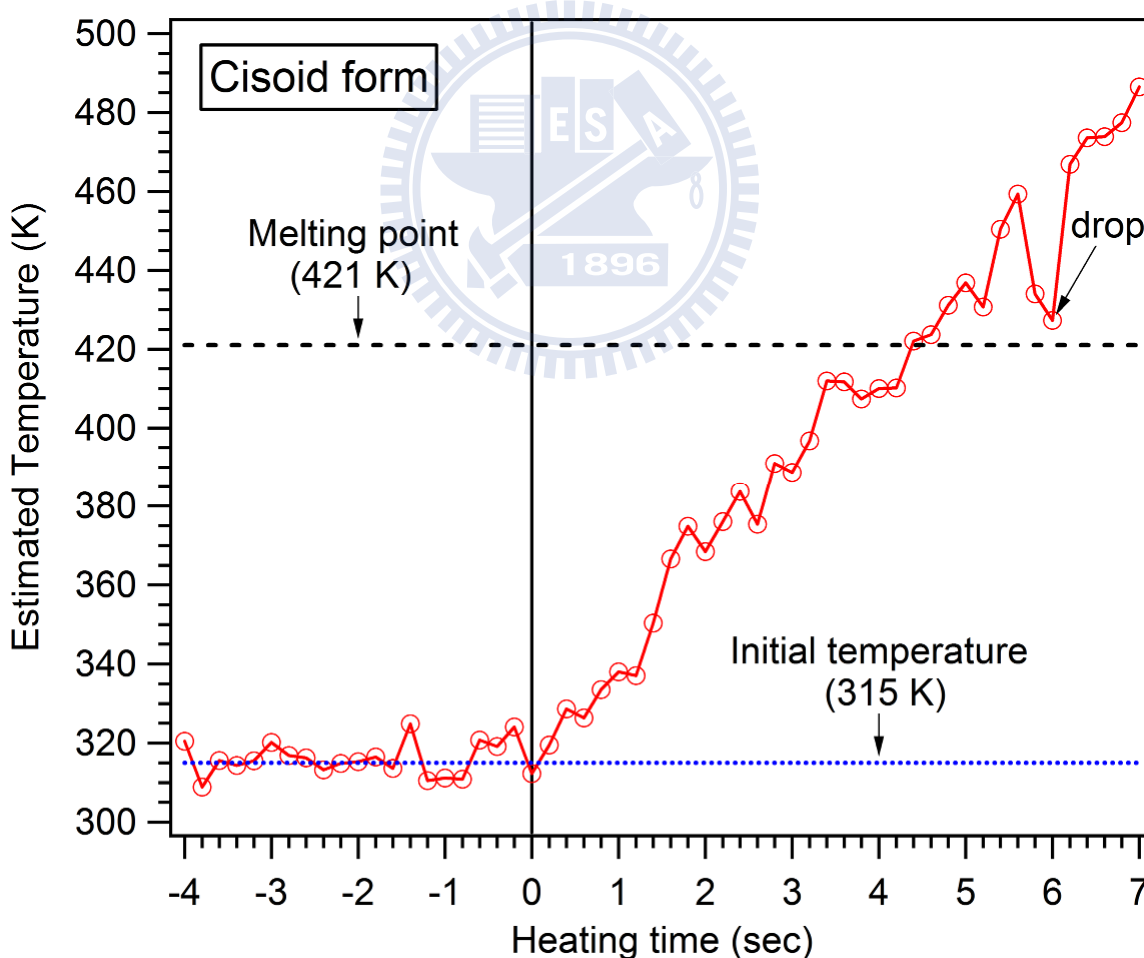


Figure III-11. Plot of the estimated temperature versus heating time for the cisoid form.

The estimation error is about ± 6 K, which is evaluated from the fluctuation before heating (<0 sec).

III-12). Figure III-12 clearly demonstrates that the DSC band (146 °C) shifts to higher temperature as the heating rate used increases. Because our heating apparatus is capable of increasing the temperature to 700 K within 30 sec, the crystal may melt at the temperature which is higher than the reported in the literature (421 K).

In the DSC result, not only the 146 °C band but also a much stronger band at 160 °C is observed when a heating rate of 5 °C/min is used. In order to confirm that our cisoid form of crystalline 1,1'-binaphthyl is pure, we performed the DSC measurement with different heating rates. We found that the relative intensity of these two bands was changed if we increase the heating rate. This means that the melting of the cisoid form takes place concomitantly with its transformation into the transoid form. This phenomenon was also reported in the literature as a solid-state process [77]. It may be related to the temperature drop around 5.6 to 6 sec shown in figure III-10. The central peak became broaden exactly at the same moment as already described in figure III-8. It is due to the fact that a rapid transformation from the melting cisoid to the transoid crystal results in an exothermic recrystallization process.

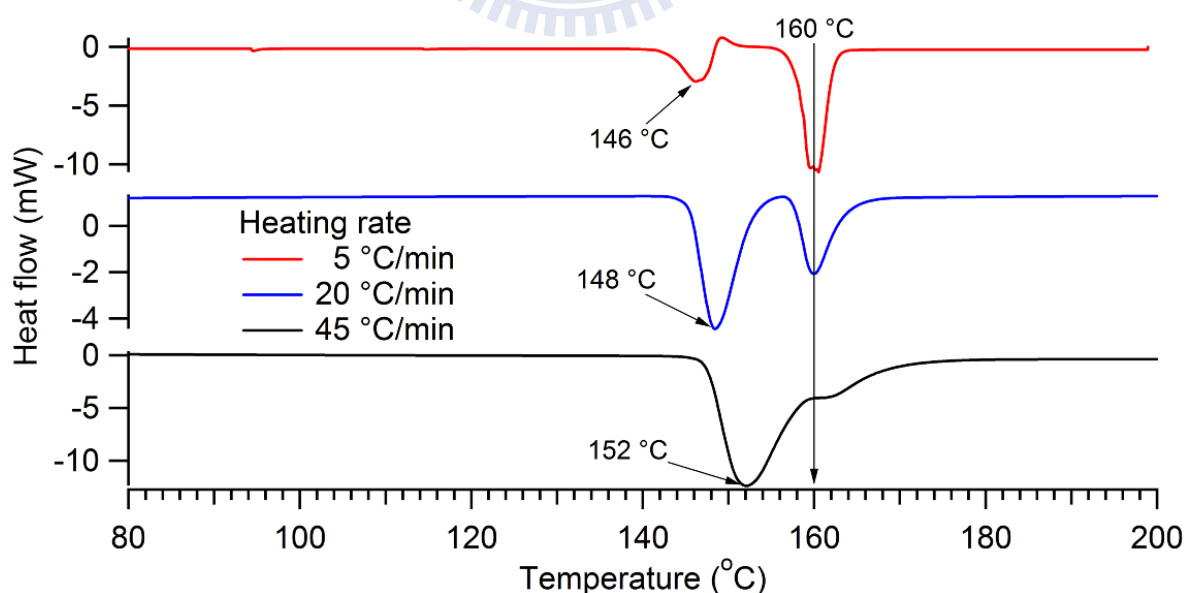


Figure III-12. Differential scanning calorimetry (DSC) measurements of cisoid form crystal with different heating rates.

Temperature change of transoid form upon heating

Figure III-13 shows a plot of the estimated temperature versus the heating time for the transoid form. The estimated temperature before heating is about 325 K, which is 10 °C higher than that of the cisoid form. The difference may be caused by different laser power (5 mW) and/or focal point of the laser on the sample. The same tendency as shown in the cisoid form is observed, the sample temperature increases rapidly to over 482 K within 7 sec heating.

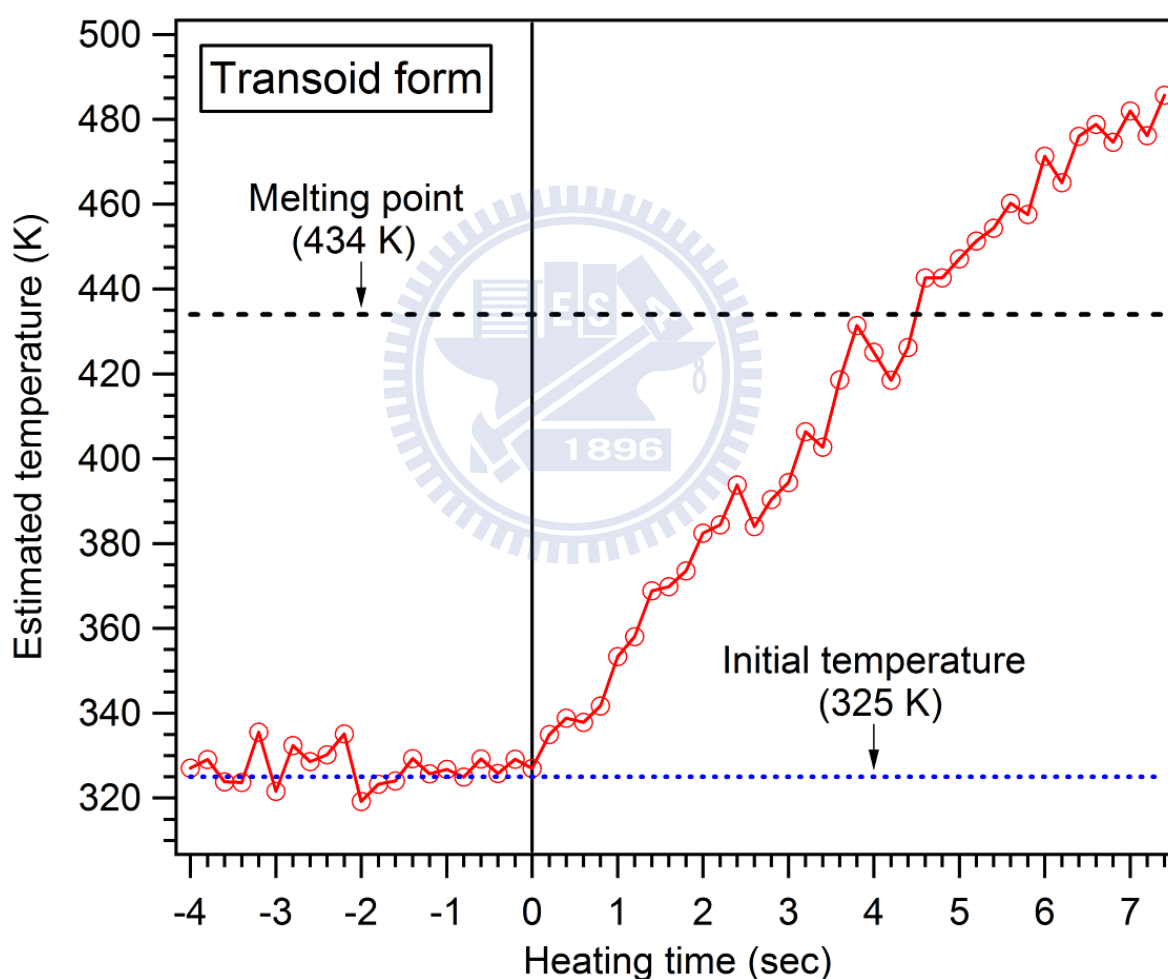


Figure III-13. Plot of the estimated temperature versus heating time for the transoid form. The estimation error is about ± 8 K, which is evaluated from the fluctuation before heating (< 0 sec).

The transoid form of 1,1'-binaphthyl, which was prepared by the procedure as described before, are highly pure. Only one DSC band is observed (figure III-14), and the DSC band (161 °C) also shifts to higher temperature as the heating rate increases. Hence, the melting point of the transoid form observed in the Raman experiment should be higher than 161 °C (434 K). However, unlike the case of the cisoid form, there is no obvious temperature drop for the transoid form (figure III-13). And the transoid conformer will not transform back to the cisoid form during heating. It is confirmed by the DSC measurement as shown in figure III-14.

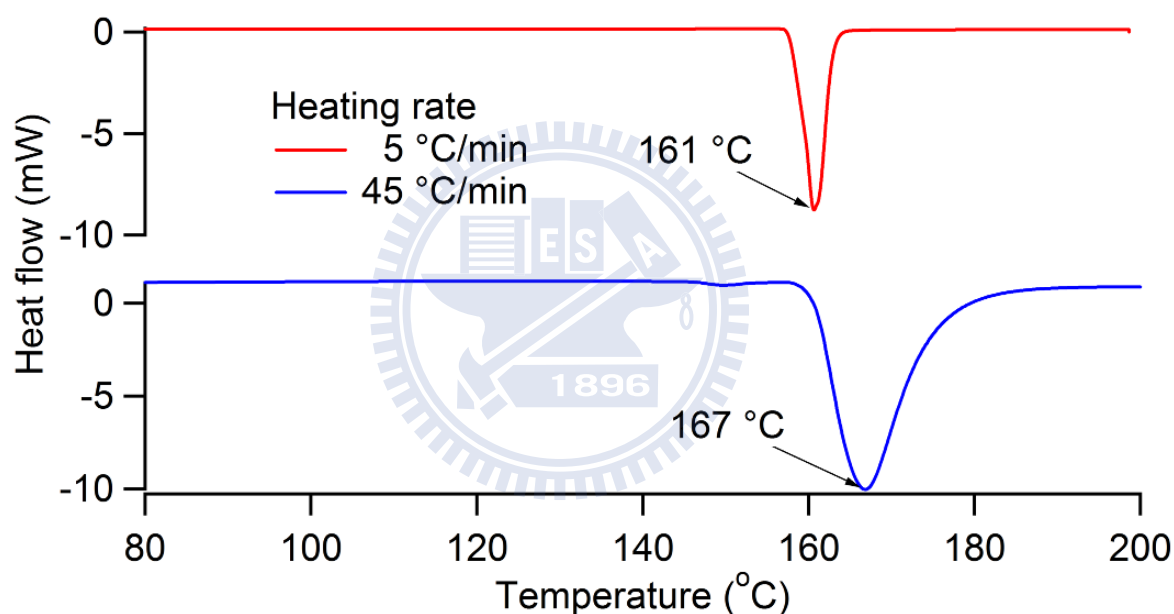


Figure III-14. Differential scanning calorimetry (DSC) measurements of transoid form crystal with different heating rates.

III-6. Discussion:

Changes in Low-frequency Raman bands change during heating

Peak position shift caused by the temperature

Figure III-15 display the changes in peak position of the low-frequency bands for the cisoid and transoid forms. The peak shifts of intramolecular vibrations such as 510 cm^{-1} and 683 cm^{-1} bands are no more than 1 cm^{-1} . Therefore, the shifts of the low-frequency Raman bands, which are larger than 1 cm^{-1} should give some special physical meanings.

A plot of peak position of low-frequency Raman bands versus temperature is shown in figure III-16. The selected range of the data points is from 0 sec to the point before melting, which are 7.4 sec for the transoid form and 5.6 sec for the cisoid form. Thus, the thermal behavior of the two crystal forms before melting can be compared. The figure seems to show linear dependence; therefore we can obtain peak positions corresponding to each temperature by simply fitting the data to a line function. The peak position at room temperature (298 K) and before melting can be derived based on the fitting function obtained. Table III-2 lists the peak shift of each low-frequency Raman band upon heating. It is known that the peak shift is related to thermal expansion of a crystal structure. We found that the Raman bands shift to a

Table III-2. The peak shift of low-frequency bands during heating

Transoid form band ($\tilde{\nu}$)	20	26	44	55	66	79	95
Peak shift (cm^{-1}) [$\tilde{\nu}(\text{T}=489)-\tilde{\nu}(\text{T}=298)$]	-1.1	-1.3	-6.2	-2.9	-3.3	-2.1	-3.8
Cisoid form band ($\tilde{\nu}$)	37	57	65	75	100	110	175
Peak shift (cm^{-1}) [$\tilde{\nu}(\text{T}=459)-\tilde{\nu}(\text{T}=298)$]	-4.6	-5.1	-5	-5.3	-6.8	-5.6	-4

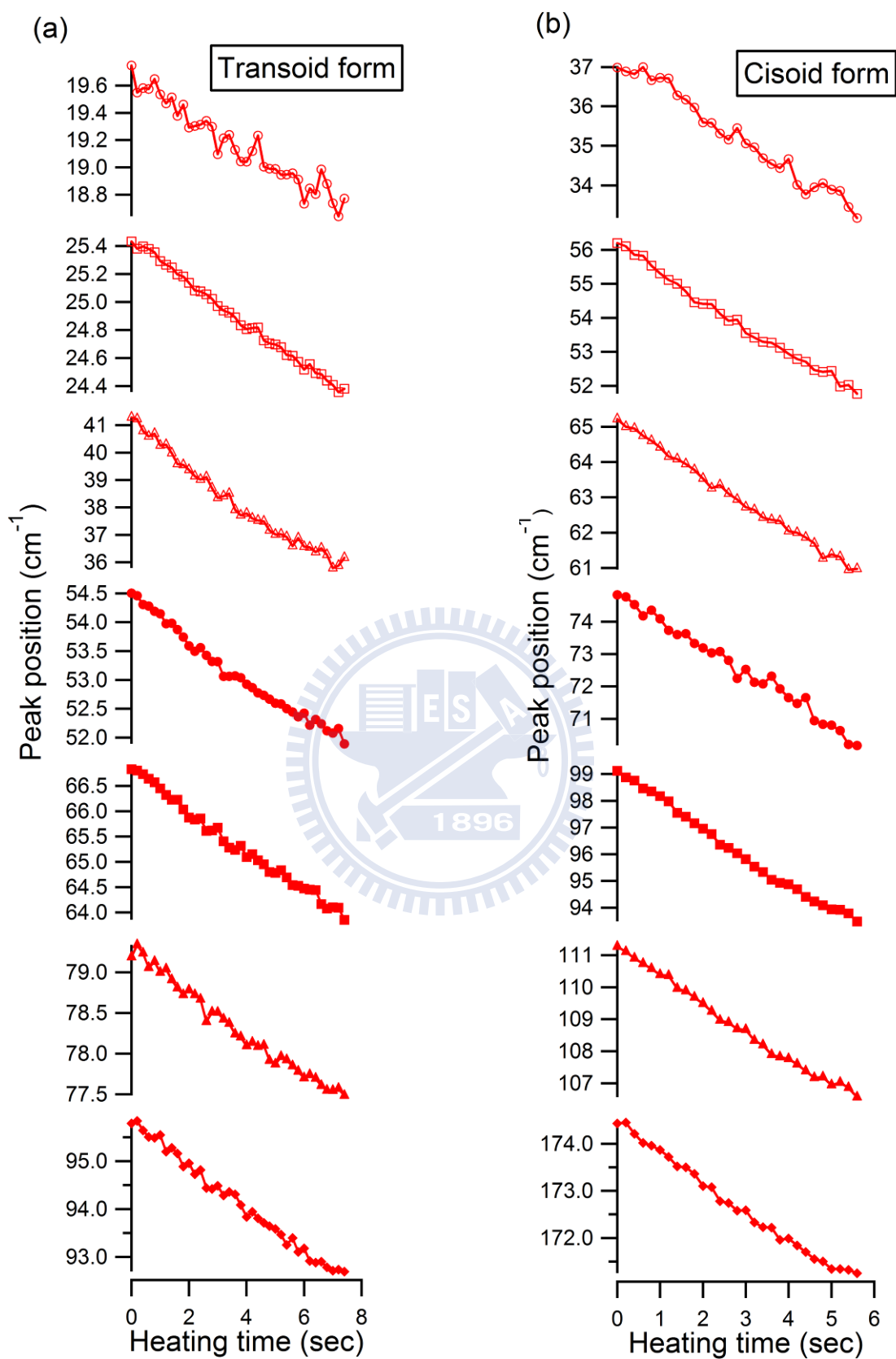


Figure III-15. Plot of the peak positions of the seven low-frequency Raman bands against heating time.

(a) Transoid form and (b) cisoid form.

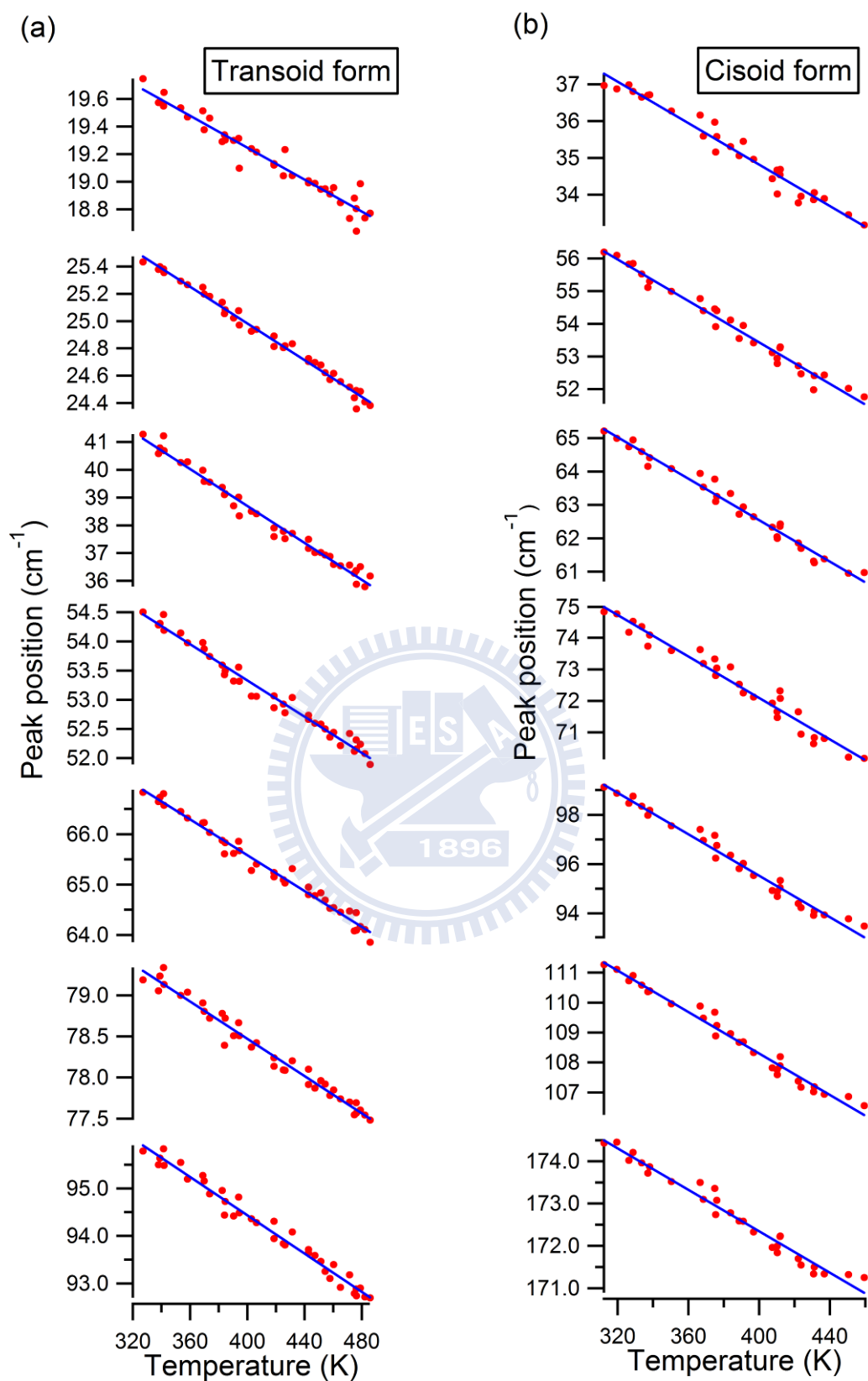


Figure III-16. Plot of the peak positions of the seven low-frequency Raman bands against estimated temperature. (a) Transoid form and (b) cisoid form. The data point and fitted results are shown in red closed circle and blue solid line, respectively.

larger extent in the cisoid form. The thermal expansion of a crystal structure makes the intermolecular interactions weaker. Therefore, the smaller shift of the Raman band found for the transoid form may imply stronger intermolecular interactions than the cisoid form if the molecular conformation does not change before melting. The crystal structure obtained from an X-ray analysis [77] (figure III-17) is consistent with this interpretation. In both cases, the intermolecular interactions are mainly of electrostatic nature, acting between the H atoms and the π electrons of the aromatic rings. In the transoid form, the molecules stack parallel to each other via the CH- π interactions, while the CH- π interactions in the cisoid form are expected to be small within each layer. Thus, the intermolecular interactions within a unit cell of the

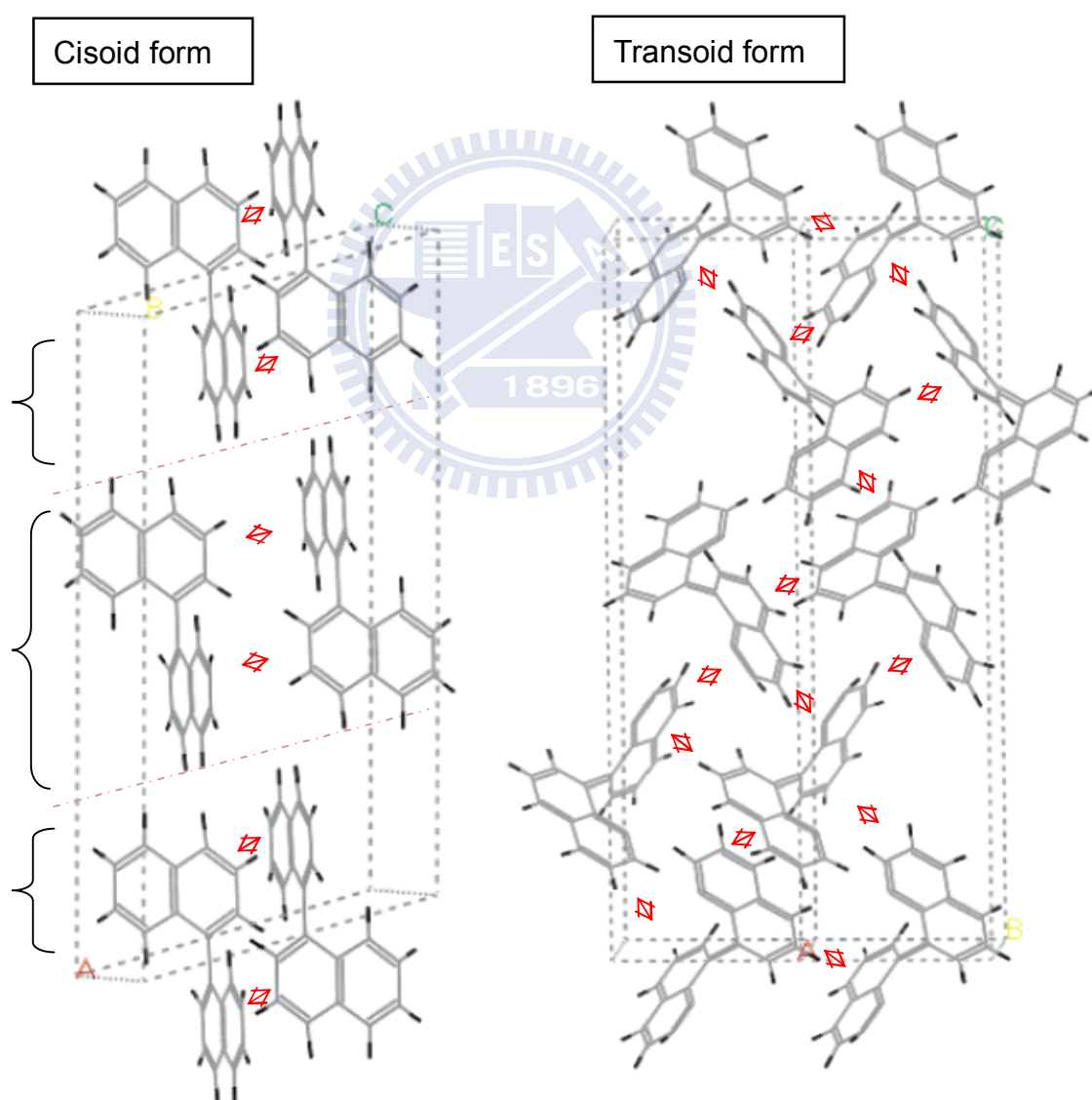


Figure III-17. The crystal structures of the two forms of 1,1'-binaphthyl.
(Taken from ref 77.)

transoid form are stronger than those in the cisoid form.

III-7. Discussion:

Possible vibrational mode of 26 cm^{-1} band in the transoid form and 100 cm^{-1} band in cisoid form

The low-frequency Raman spectra of both conformers of 1,1'-binaphthyl have not been reported before. Our research goal is to understand why they show such distinct spectral features, although it is difficult to fully assign each low-frequency Raman band at the present stage. The most interesting is probably the fact that the 26 cm^{-1} band is quite strong for the transoid conformer but not observed for the cisoid form. It is also interesting that the most intense band of the cisoid form at $\sim 100\text{ cm}^{-1}$ appears as a doublet band (see figure III-6). Based on the present data and theoretical results, we propose a possible assignment of these quite strong low frequency vibrational bands.

As shown in figure III-7, we found that the band shape of the doublet band at 100 cm^{-1} is still observed at 6.0 sec, while the sample has melted already judging from the central band broadening. In contrast to this band, the band shape of other low-frequency bands cannot be clearly seen. We found the same tendency at the 26 cm^{-1} of the transoid form. In principle, a lattice vibration will lose its band intensity and band shape when the crystal structure no longer exists. Thus, we attribute the 26 cm^{-1} band of the transoid form to an intramolecular vibration rather than to a lattice vibration. From density functional theory (DFT) calculation results, 1,1'-binaphthyl in the gas phase shows three intramolecular vibrational bands at 17, 58, and 61 cm^{-1} . The 17 cm^{-1} band is assigned to be C–C torsional vibration, the other two are out-of-plane deformations of two naphthyl moieties like twisting and wagging motions as shown in figure III-18. Therefore, it is highly likely that the 26 cm^{-1} in the transoid form is

assigned to the torsional motion. The calculated out-of-plane deformations might be the doublet band in the cisoid conformer.

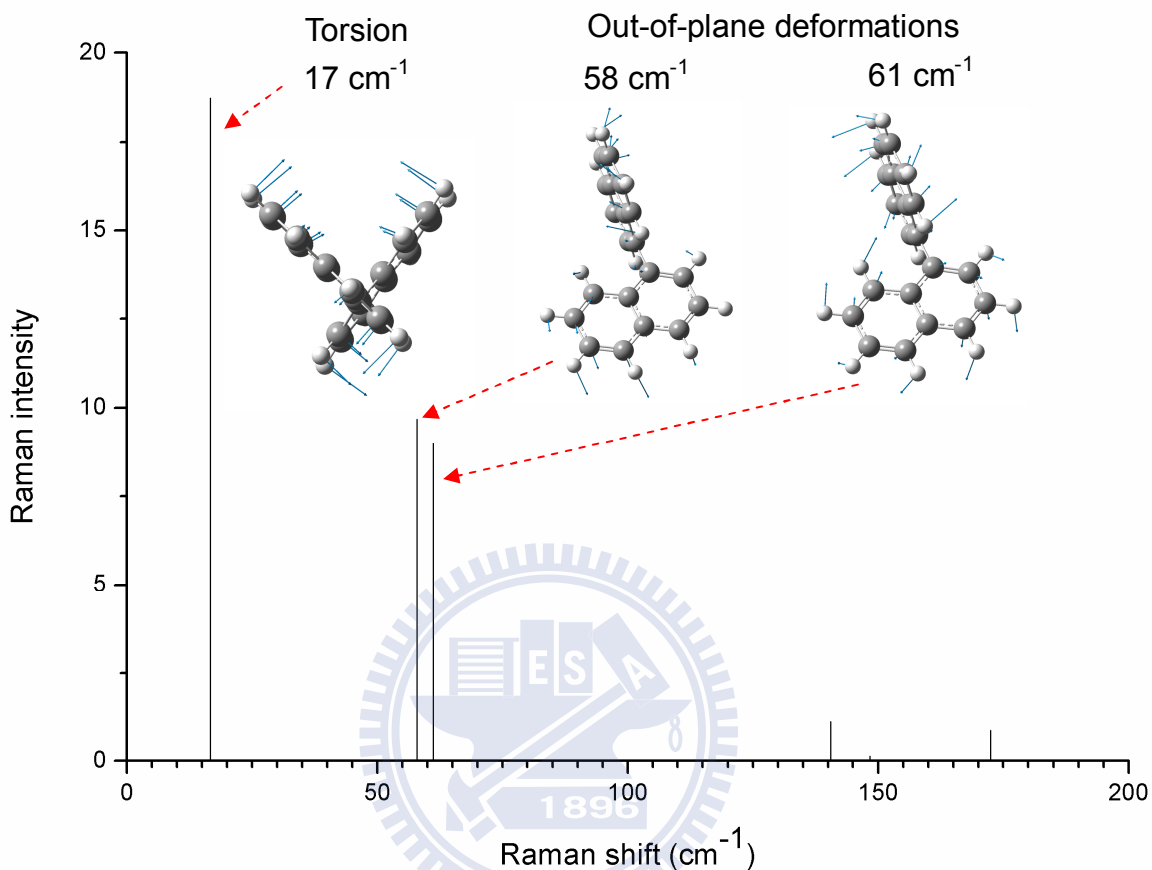


Figure III-18. The intramolecular vibrations in gas phase 1,1'-binaphthyl molecule calculated from density functional theory. (Method: DFT/B3LYP; Basis set: 6-311G ++(d, p))

The interatomic distances between $\text{H}(8) \cdots \text{H}(8')$, $\text{C}(1) \cdots \text{H}(2')$ and $\text{C}(1) \cdots \text{H}(8')$ of 1,1'-binaphthyl has been determined from X-ray analysis [62], which are closely related to the spectral feature at 26 cm^{-1} (torsional motion) in the transoid form and the doublet band at 100 cm^{-1} in the cisoid form. The $\text{H}(8) \cdots \text{H}(8')$ distances are 2.81 \AA and 3.03 \AA for the cisoid and transoid forms, respectively. Because of the shorter $\text{H}(8) \cdots \text{H}(8')$ distance, the torsional motion (in-plane vibration) in the cisoid form may be restricted, possibly resulting in the apparent absence of the torsional band at 26 cm^{-1} in the cisoid form. On the other hand, the band intensity of out-of-plane vibrations of 1,1'-binaphthyl are related to the distances of

C(1)···H(2') and C(1)···H(8'), which are 2.67 Å and 2.62 Å in the cisoid form and 2.65 Å and 2.59 Å in the transoid form, respectively. Since the distances of C(1)···H(2') and C(1)···H(8') are slightly longer in the cisoid form, out-of-plane deformations in the cisoid form are relatively easily achieved and may give rise to a quite strong band.

III-8. Torsional motions of other crystalline aromatic compounds

As mentioned in the introduction part of this chapter, large amplitude motions such as C–C torsional motion in biphenyl give a strong Raman intensity. The transoid 1,1'-binaphthyl in the present study can also be interpreted by the same reasoning. In the course of our study, we have found that some other molecules which have two polyaromatic rings connected by a σ -bond (either C–C or C–N single bond) show similar tendency. Their low-frequency Raman spectra are compared in figure III-19. Since these compounds are heavier than 1,1'-binaphthyl, the frequency of their torsional vibration (indicated in the figure) should be lower than the value for 1,1'-binaphthyl (26 cm^{-1}). This is the case, as can be seen from figure III-19. In addition, transoid 1,1'-binaphthyl and these four compounds show similar spectral features in the range of $40\text{--}120\text{ cm}^{-1}$. These low-frequency Raman bands couple to each other and produce a high offset. From their crystal structures [77], we suppose that the coupling and high offsets might be due to π – π interactions between polyaromatic rings of neighboring molecules because the adjacent heavy rings stack in parallel to each other. These π – π interactions are intermolecular van der Waals-like attractive forces. The energy gap due to the π – π interactions is typically smaller than that of intramolecular vibrations ($200\text{--}4000\text{ cm}^{-1}$). Therefore, the Raman shift of such interactions appears in the low-frequency region ($<200\text{ cm}^{-1}$). Furthermore, they split into a few peaks coupling to each other. We suspect that the Raman bands at 44, 55, 66, 79, and 95 cm^{-1} come from the same intermolecular interactions.

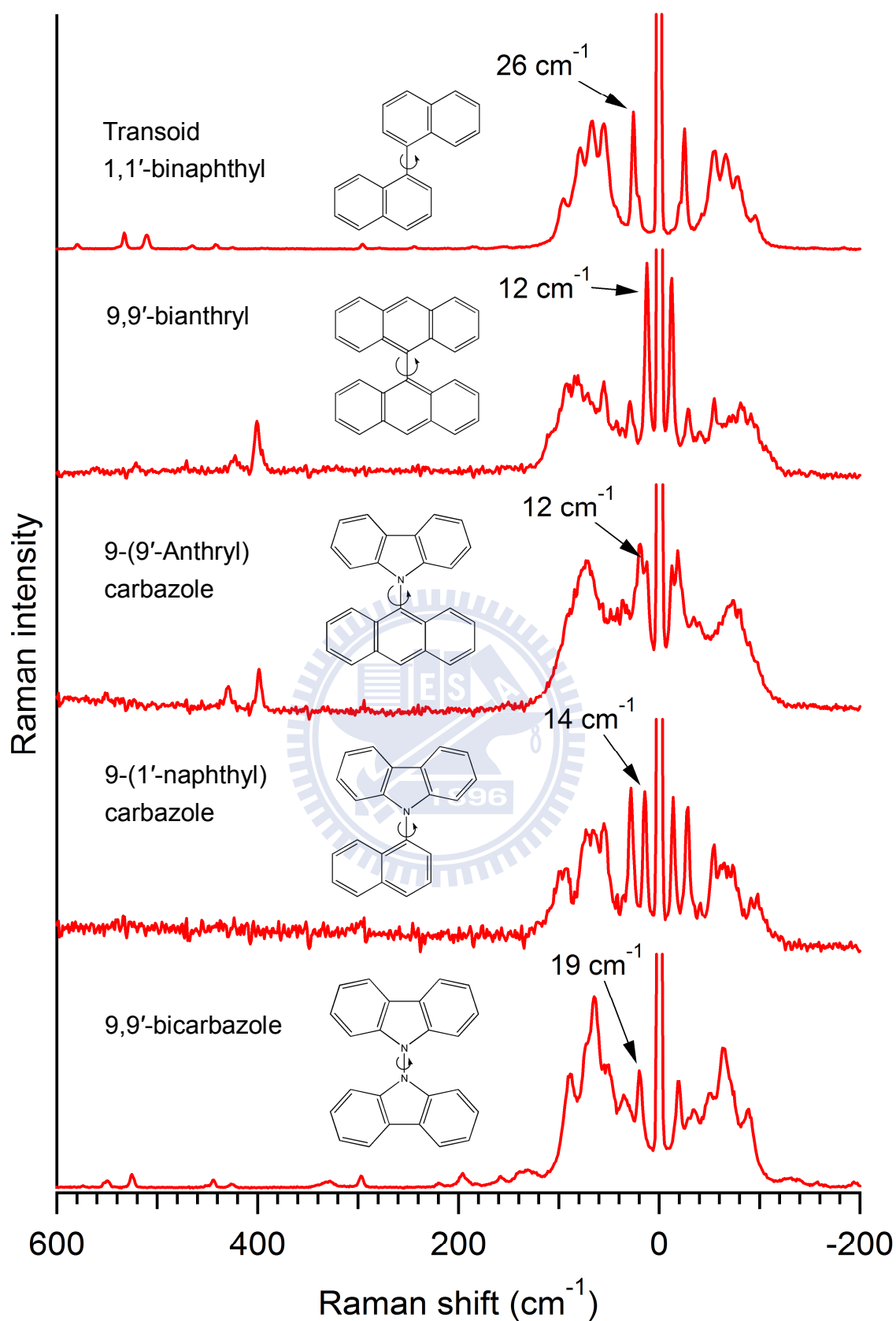


Figure III-19. Raman spectra of aromatic compounds containing the torsional motion.

Chapter IV

Conclusion



The constructed multichannel low-frequency Raman spectrometer with an I₂-vapor containing cell as a Rayleigh rejection filter has been described. The iodine vapor filter has high Rayleigh scattering elimination efficiency, enabling us to measure Raman spectra down to $\pm 5\text{ cm}^{-1}$ in both Stokes and anti-Stokes sides simultaneously. In addition, a wide spectral range (-200 – $+1100\text{ cm}^{-1}$) can be recorded without resort to scanning the grating of a spectrograph. Thanks to the high spectral reproducibility of the multichannel detection, the superfluous artifacts caused by the I₂ vapor absorption are reduced to a negligible level just by using a simple and straightforward intensity correction method. Compared with existing metal vapor filters, the iodine vapor filter has a much narrower elimination bandwidth, free from complexity of adding fluorescence quenching gases.

We utilized the constructed Raman spectrometer to investigate the two crystal polymorphs of 1,1'-binaphthyl, a building block of the chiral catalyst. The Raman spectra of these two crystal forms showed distinct features in the low-frequency region ($<200\text{ cm}^{-1}$), but no apparent difference was observed above 200 cm^{-1} . Not only lattice vibrations but also intramolecular vibrations were observed in the low-frequency region. The most intense intramolecular vibrational band at 26 cm^{-1} of the transoid form was associated with the torsional motion around the interring C–C single bond, whereas the doublet peak around 100 cm^{-1} was assigned to be out-of-plane deformations. The torsional motion and out-of-plane vibration of 1,1'-binaphthyl were found to correlate with the interatomic distances between H(8)···H(8'), C(1)···H(2'), and C(1)···H(8'). With a better spectral resolution and polarized Raman measurements, it will be possible to assign each low-frequency Raman band of both forms of crystalline 1,1'-binaphthyl.

Real-time tracing of the melting process of the cisoid and transoid forms was done with rapid heating. A series of Raman spectra were recorded every 0.2 sec. Crystal structure loss manifested by spectral changes was seen in the low-frequency region. There remained the 26

cm^{-1} band of the transoid form and the 100 cm^{-1} band of the cisoid form even after melting. This observation agrees with our prediction that these two bands arise from intramolecular vibrations rather than lattice vibrations. In addition, the sample temperature was determined by the Stokes/anti-Stokes intensity ratio. Seven symmetrized Lorentz functions convoluted with the Bose–Einstein factor were used to fit the low-frequency Raman spectra in both cisoid and transoid forms. Based on the high-quality fitted results, the sample temperature was determined to a high accuracy. The peak position of each low-frequency band was also determined and their change with temperature was discussed. Peak shifts due to thermal expansion in the transoid form were found to be smaller than those in the cisoid form. Thus, intermolecular interactions in the transoid form are supposed to be stronger than those in the cisoid form. It is consistent with the X-ray crystal structure reported in the literature.

As demonstrated in the present study, real-time tracing of solid samples with fast multichannel low-frequency Raman spectroscopy is a powerful and informative approach to phase transitions. A wealth of information on intermolecular interactions can be obtainable by using this technique. Bearing the advantages of low cost and short measurement time, our Raman apparatus provides deeper insights into the dynamical aspects of molecules compared with X-ray crystallography. If a faster read-out time detector is employed such as electron multiplying charge coupled device (EMCCD), it would be more helpful for understanding condensed phase dynamics.

References



- [1] M. E. Fisher, "The theory of equilibrium critical phenomena," *Reports on Progress in Physics*, vol. 30, pp. 615-730, 1967.
- [2] H. E. Stanley, *Introduction to phase transitions and critical phenomena*. New York: Oxford Univ. Press, 1971.
- [3] M. Born and K. Huang, *Dynamical theory of crystal lattices*: Oxford : Clarendon Press, 1954.
- [4] R. Loudon, "The Raman effect in crystals," *Advances in Physics*, vol. 50, pp. 813-864, 2001.
- [5] S. P. S. Porto, P. A. Fleury, and T. C. Damen, "Raman Spectra of TiO_2 , MgF_2 , ZnF_2 , FeF_2 , and MnF_2 ," *Physical Review*, vol. 154, pp. 522-526, 1967.
- [6] G. E. Walrafen, "Raman Spectral Studies of Water Structure," *The Journal of Chemical Physics*, vol. 40, pp. 3249-3256, 1964.
- [7] J. Loader, *Basic laser Raman spectroscopy*. London: Sadtler Research Laboratories, 1970.
- [8] Q. Zhong and J. T. Fourkas, "Optical Kerr Effect Spectroscopy of Simple Liquids," *Journal of Physical Chemistry*, vol. 112, pp. 15529-15539, 2008.
- [9] Y. J. Chang and E. W. Castner, "Intermolecular Dynamics of Substituted Benzene and Cyclohexane Liquids, Studied by Femtosecond Nonlinear-Optical Polarization Spectroscopy," *Journal of Physical Chemistry*, vol. 100, pp. 3330-3343, 1996.
- [10] M. C. Beard, G. M. Turner, and C. A. schmittenmaer, "Terahertz Spectroscopy," *The Journal of Physical Chemistry B*, vol. 106, pp. 7146-7159, 2002.
- [11] J. L. Wood, "Far-infrared spectroscopy," *Quarterly Reviews, Chemical Society*, vol. 17, pp. 362-380, 1963.
- [12] B. Hehlen, E. Courtens, R. Vacher, A. Yamanaka, M. Kataoka, and K. Inoue, "Hyper-Raman Scattering Observation of the Boson Peak in Vitreous Silica," *Physical Review Letters*, vol. 84, pp. 5355-5358, 2000.
- [13] K. Inoue and S. Akimoto, "Hyper-Raman scattering spectra in the low frequency range in cubic BaTiO_3 and the mechanism of the phase transition," *Solid State Communications*, vol. 46, pp. 441-445, 1983.
- [14] H. Vogt, M. D. Fontana, G. E. Kugel, and P. Gunter, "Low-frequency dielectric response in cubic KNbO_3 studied by hyper-Raman scattering," *Physical Review B*, vol. 34, p. 410, 1986.
- [15] B. Hehlen, E. Courtens, A. Yamanaka, and K. Inoue, "Nature of the Boson peak of silica glasses from hyper-Raman scattering," *Journal of Non-Crystalline Solids*, vol. 307, p. 87, 2002.
- [16] S. W. Lovesey, *Dynamics of Solids and Liquids by Neutron Scattering*. Berlin; New York: Springer-Verlag, 1977.
- [17] H. O. Hamaguchi, "Calibrating Multichannel Raman Spectrometers," *Applied*

- Spectroscopy Reviews*, vol. 24, pp. 137-174, 1988.
- [18] J. Barbillat, B. Roussel, and E. D. Silva, "Use of Multi-notch Filter for Simultaneous Recording of Stokes and Anti-Stokes Raman Signals Close to the Exciting Line," *Journal of Raman Spectroscopy*, vol. 30, pp. 745-755, 1999.
 - [19] G. J. Puppels, C. G. d. Grauw, M. B. J. t. Plate, and J. Greve, "Chevron-Type Dielectric Filter Set for Efficient Narrow-Band Laser Line Rejection in Raman Microspectrometers," *Applied Spectroscopy* vol. 48, pp. 1399-1402, 1994.
 - [20] D. J. Dunstan and M. D. Frogley, "Double subtractive spectrometer as a tunable high-resolution broad-bandpass optical filter," *Review of Scientific Instruments*, vol. 73, pp. 3742-3746, 2002.
 - [21] F. Rasetti, "Raman Spectra of Crystals," *Nature*, vol. 127, pp. 626-627, 1931.
 - [22] H. Shimizu, S. A. Lee, and C. Y. She, "High spectral resolution lidar system with atomic blocking filters for measuring atmospheric parameters," *Applied Optics*, vol. 22, pp. 1373-1381, 1983.
 - [23] S. H. Bloom, R. Kremer, P. A. Searcy, M. Rivers, J. Menders, and E. Korevaar, "Long-range, noncoherent laser Doppler velocimeter," *Optics Letters*, vol. 16, p. 1794, 1991.
 - [24] G. E. Devlin, J. L. Davis, L. Chase, and S. Geschwind, "Absorption of Unshifted Scattered Light by a Molecular I₂ Filter in Brillouin and Raman Scattering," *Applied Physics Letters*, vol. 19, pp. 138-141, 1971.
 - [25] J. R. Scherer, "Removal of I₂ absorption lines from 514-nm excited raman spectra," *Applied Optics*, vol. 17, pp. 1621-1623, 1978.
 - [26] P. E. Schoen and D. A. Jackson, "The iodine filter in Raman and Brillouin spectroscopy," *journal of Physics E: Scientific Instruments*, vol. 5, pp. 519-521, 1972.
 - [27] L. Laughman, L. W. Davis, and T. Nakamura, "Raman-Scattering Line Shape of the Soft E Polariton Mode in BaTiO₃," *Physical Review B*, vol. 6, pp. 3322-3326, 1972.
 - [28] K. F. Wall and R. K. Chang, "Separation of the low-frequency mode from the inelastic continuum scattering of a sers active electrode," *Chemical Physics Letters*, vol. 129, pp. 144-148, 1986.
 - [29] K. F. Wall, M. L. A. Temperini, and R. K. Chang, "Potential-dependent measurements of the low-frequency mode, the inelastic continuum, elastic scattering and sers from a Ag electrode," *Chemical Physics Letters*, vol. 129, p. 253, 1986.
 - [30] K. F. Wall and R. K. Chang, "I₂-vapor notch filter with optical multichannel detection of low-frequency-shift inelastic scattering from surface-enhanced Raman-scattering active electrodes," *Optics Letters*, vol. 11, pp. 493-495, 1986.
 - [31] H. Okajima and H. O. Hamaguchi, "Fast Low Frequency (Down to 10 cm⁻¹) Multichannel Raman Spectroscopy Using an Iodine Vapor Filter," *Applied Spectroscopy*, vol. 63, pp. 958-960, 2009.

- [32] R. B. Miles, A. P. Yalin, Z. Tang, S. H. Zaidi, and J. N. Forkey, "Flow field imaging through sharp-edged atomic and molecular 'notch' filters," *Measurement Science and Technology*, vol. 12, pp. 442-451, 2001.
- [33] G. S. Elliott, N. Glumac, and C. D. Carter, "Molecular filtered Rayleigh scattering applied to combustion," *Measurement Science and Technology*, vol. 12, p. 452, 2001.
- [34] M. Esselborn, M. Wirth, A. Fix, M. Tesche, and G. Ehret, "Airborne high spectral resolution lidar for measuring aerosol extinction and backscatter coefficients," *Applied Optics*, vol. 47, pp. 346-358, 2008.
- [35] J. Bood, P.-E. Bengtsson, and M. A. n, "Stray Light Rejection in Rotational Coherent Anti-Stokes Raman Spectroscopy by use of a Sodium-Seeded Flame," *Applied Optics*, vol. 37, pp. 8392-8396, 1998.
- [36] M. J. Pelletier, "Potassium Vapor Near-IR Laser Line Rejection Filter for Raman Spectroscopy," *Applied Spectroscopy*, vol. 47, pp. 69-74, 1993.
- [37] R. Indralingam, J. B. Simeonsson, G. A. Petrucci, B. W. Smith, and J. D. Winefordner, "Raman spectrometry with metal vapor filters," *Analytical Chemistry*, vol. 64, pp. 964-967, 1992.
- [38] P. J. Horoyski and M. L. W. Thewalt, "Fourier Transform Raman and Brillouin Spectroscopy Using Atomic Vapor Filters," *Applied Spectroscopy*, vol. 48, pp. 843-847, 1994.
- [39] A. Nohe, G. LeTmanna, H. Schwoerera, W. Kiefer, J. Sawatzkib, and G. Surawiczb, "High resolution low wavenumber Fourier transform Raman spectroscopy with a rubidium vapor filter and a Ti sapphire laser," *Journal of Molecular Structure*, vol. 410, pp. 65-68, 1997.
- [40] W. L. Peticolas, "INELASTIC LIGHT SCATTERING AND THE RAMAN EFFECT," *Annual Review of Physical Chemistry*, vol. 23, pp. 93-116, 1972.
- [41] R. S. Mulliken, "Iodine Revisited," *The Journal of Chemical Physics*, vol. 55, p. 288, 1971.
- [42] I. J. McNaught, "The electronic spectrum of iodine revisited," *Journal of Chemical Education*, vol. 57, pp. 101-105, 1980.
- [43] J. P. Hohimer, R. C. Kelly, and F. K. Tittel, "Frequency Stabilization of a High Power Argon Laser," *Applied Optics*, vol. 11, pp. 626-629, 1972.
- [44] F. Spieweck, "¹²⁷I₂-Absorption bei 3 Kr II-Laserlinien," *Metrologia*, vol. 9, pp. 24-25, 1973.
- [45] A. J. Wallard, "The frequency stabilization of gas lasers," *Journal of Physics E: Scientific Instruments*, vol. 6, pp. 793-807, 1973.
- [46] J. D. Knox and Y.-H. Pao, "High-Resolution Saturation Spectra of the Iodine Isotope I₂¹²⁹ in the 633-nm Wavelength Region," *Applied Physics Letters*, vol. 18, pp. 360-361, 1971.

- [47] C. R. Hanes and C. E. Dahlstrom, "Iodine Hyperfine Structure Observed in Saturated Absorption at 633 nm," *Applied Physics Letters*, vol. 14, p. 362, 1969.
- [48] J. L. Hall, L.-S. Ma, M. Taubman, B. Tiemann, F.-L. Hong, O. Pfister, and J. Ye, "Stabilization and Frequency Measurement of the Iastabilized Nd: YAG laser," *IEEE Transactions on Instrumentation and Measurement*, vol. 48, pp. 583-586, 1999.
- [49] F. Hong, "Frequency reproducibility of an iodine-stabilized Nd:YAG laser at 532 nm," *Optics Communications*, vol. 235, pp. 377-385, 2004.
- [50] D. R. Stull, "Vapor Pressure of Pure Substances. Organic and Inorganic Compounds," *Industrial & Engineering Chemistry*, vol. 39, p. 517, 1947.
- [51] J. R. Ferraro, K. Nakamoto, and C. W. Brown, *Introductory Raman Spectroscopy*. New York: Oxford Academic Press, 2003.
- [52] W. Kiefer and H. J. Bernstein, "Vibrational-Rotational Structure in the Resonance Effect of Iodine Vapor," *Journal of Molecular Structure*, vol. 43, pp. 366-381, 1972.
- [53] R. Noyori and H. Takaya, "BINAP: an efficient chiral element for asymmetric catalysis," *Accounts of Chemical Research*, vol. 23, pp. 345-350, 1990.
- [54] D. J. Cram, R. C. Helgeson, K. Koga, E. P. Kyba, K. Madan, L. R. Sousa, M. G. Siegel, P. Moreau, and G. W. Gokel, "Host-guest complexation. 9. Macrocyclic polyethers and sulfides shaped by one rigid dinaphthyl unit and attached arms. Synthesis and survey of complexing abilities," *The Journal of Organic Chemistry*, vol. 43, pp. 2758-2772, 1978.
- [55] A. Miyashita, A. Yasuda, H. Takaya, K. Toriumi, T. Ito, T. Souchi, and R. Noyori, "Synthesis of 2,2'-bis(diphenylphosphino)-1,1'-binaphthyl (BINAP), an atropisomeric chiral bis(triaryl)phosphine, and its use in the rhodium(I)-catalyzed asymmetric hydrogenation of .alpha.-(acylamino)acrylic acids," *Journal of the American Chemical Society*, vol. 102, pp. 7932-7934, 1980.
- [56] A. Almenningen, O. Bastiansen, L. Fernholt, B. N. Cyvin, S. J. Cyvin, and S. Samdal, "Structure and barrier of internal rotation of biphenyl derivatives in the gaseous state : Part 1. The molecular structure and normal coordinate analysis of normal biphenyl and pedeuterated biphenyl," *Journal of Molecular Structure*, vol. 128, pp. 59-76, 1985.
- [57] A. S. Cooke and M. M. Harris, "Ground-state strain and other factors influencing optical stability in the 1,1'-binaphthyl series," *Journal of the Chemical Society (Resumed)*, pp. 2365-2373, 1963.
- [58] Richard E. Pincock, Robert R. Perkins, Alan S. Ma, and K. R. Wilson, "Probability Distribution of Enantiomorphous Forms in Spontaneous Generation of Optically Active Substances," *Science*, vol. 174, pp. 1018-1020, 1971.
- [59] Y. Badar, C. C. K. Ling, A. S. Cooke, and M. M. Harris, "Two Crystalline Modifications of 1,1'-Binaphthyl," *Journal of the Chemical Society*, pp. 1543-1544, 1965.

- [60] W. A. C. Brown, J. Trottera, and J. M. Robertson, "X-Ray Study of Crystals isolated during the Synthesis of 1,12-o-Phenyleneperylene," *Proceedings of the Chemical Society*, pp. 115-116, 1961.
- [61] K. A. Kerr and J. M. Robertson, "Crystal and Molecular Structure of 1,1'-Binaphthyl," *Journal of the Chemical Society B*, pp. 1146-1149, 1969.
- [62] R. B. Kress, E. N. Duesler, M. C. Etter, I. C. Paul, and D. Y. Curtin, "Solid-state Resolution of Binaphthyl: Crystal and Molecular Structures of the Chiral (A)¹ Form and Racemic (B)¹ Form and the Study of the Rearrangement of Single Crystals. Requirements for Development of Hemihedral Faces for Enantiomer Identification," *Journal of the American Chemical Society*, vol. 102, pp. 7709-7714, 1980.
- [63] C. V. Shank, E. P. Ippen, O. Teschke, and K. B. Eisenthal, "Picosecond dynamics of conformational changes in 1,1'-binaphthyl," *The Journal of Chemical Physics*, vol. 67, pp. 5547-5551, 1977.
- [64] R. A. Friedel, M. Orchin, and L. Reggel, "Steric Hindrance and Short Wave Length Bands in the Ultraviolet Spectra of Some Naphthalene and Diphenyl Derivatives," *Journal of the American Chemical Society*, vol. 70, pp. 199-204, 1948.
- [65] R. M. Hochstrasser, "THE EFFECT OF INTRAMOLECULAR TWISTING ON THE EMISSION SPECTRA OF HINDERED AROMATIC MOLECULES: PART I. 1,1'-BINAPHTHYL," *Canadian Journal of Chemistry*, vol. 39, pp. 459-470, 1961.
- [66] M. J. Riley, A. R. Lacey, M. G. Sceats, and R. G. Gilbert, "LOW-TEMPERATURE VIBRONIC SPECTRA OF 1,1'-BINAPHTHYL," *Journal of Chemical Physics*, vol. 72, pp. 83-91, 1982.
- [67] A. R. Lacey and F. J. Craven, "A preliminary study of the conformation of 1,1'-binaphthyl in solution by Raman spectroscopy," *Chemical Physics Letters*, vol. 126, pp. 589-592, 1986.
- [68] S. Fujiyoshi, S. Takeuchi, and T. Tahara, "Time-Resolved Impulsive Stimulated Raman Studies of 1,1'-Binaphthyl in the Excited State: Low-Frequency Vibrations and Conformational Relaxation," *The Journal of Physical Chemistry A*, vol. 108, pp. 5938-5943, 2004.
- [69] V. Liégeois, "A Vibrational Raman Optical Activity Study of 1,1'-Binaphthyl Derivatives," *ChemPhysChem*, vol. 10, pp. 2017-2025, 2009.
- [70] F. Zhang, G. B. Bacskay, and S. H. Kable, "Quantum Chemical Determination of the Equilibrium Geometries and Harmonic Vibrational Frequencies of 1,1'-, 1,2'- and 2,2'-Binaphthyl in Their Ground and Excited (1La) Electronic States," *The Journal of Physical Chemistry A*, vol. 108, pp. 172-184, 2003.
- [71] K. Gustav, J. Sühnel, and U. P. Wild, "Theoretical study on geometry and spectroscopic properties of 1,1'-binaphthyl in the electronic ground and first excited singlet states," *Chemical Physics*, vol. 31, pp. 59-65, 1978.

- [72] R. W. Bigelow and R. W. Anderson, "A CNDO/S study on the electronic structure of 1,1'-binaphthyl," *Chemical Physics Letters*, vol. 58, pp. 114-118, 1978.
- [73] M. F. M. Post, J. K. Eweg, J. Langelaar, J. D. W. van Voorst, and G. Ter Maten, "SCF Cl calculations and assignment of the S1 \rightarrow S₀ absorption spectra of 1,1'-binaphthyl in different molecular conformations," *Chemical Physics*, vol. 14, pp. 165-176, 1976.
- [74] R. E. Carter and T. Liljefors, "A theoretical study of configurational inversion of 1,1'-binaphthyl by molecular mechanics," *Tetrahedron*, vol. 32, pp. 2915-2922, 1976.
- [75] A. Gamba, E. Rusconi, and M. Simonetta, "A conformational study of phenyl- and naphthyl-naphthalenes," *Tetrahedron*, vol. 26, pp. 871-877, 1970.
- [76] H. Takeuchi, S. Suzuki, A. J. Dianoux, and G. Allen, "Low frequency vibrations in crystalline biphenyl: Model calculations and raman and neutron spectra," *Chemical Physics*, vol. 55, pp. 153-162, 1981.
- [77] C. I. Sainz-Díaz, A. P. Martín-Islán, and J. H. E. Cartwright, "Chiral Symmetry Breaking and Polymorphism in 1,1'-Binaphthyl Melt Crystallization," *The Journal of Physical Chemistry B*, vol. 109, pp. 18758-18764, 2005.
- [78] D. K. Kondepudi, J. Laudadio, and K. Asakura, "Chiral Symmetry Breaking in Stirred Crystallization of 1,1'-Binaphthyl Melt," *Journal of the American Chemical Society*, vol. 121, pp. 1448-1451, 1999.
- [79] R. Shuker and R. W. Gammon, "Raman-Scattering Selection-Rule Breaking and the Density of States in Amorphous Materials," *Physical Review Letters*, vol. 25, pp. 222-225, 1970.